# Role of graphene/metal oxide composites as photocatalysts, adsorbents and disinfectants in water treatment: a review

Ravi Kant Upadhyay,[a] Navneet Soin[b] and Susanta Sinha Roy*[c]

With a rapidly growing population, development of new materials, techniques and devices which can provide safe potable water continues to be one of the major research emphases of the scientific community. While the development of new metal oxide catalysts is progressing, albeit at a slower pace, the concurrent and rapid development of high surface area catalyst supports such as graphene and its functionalised derivatives has provided unprecedented promise in the development of multifunctional catalysts. Recent works have shown that metal oxide/graphene composites can perform multiple roles including (but not limited to): photocatalysts, adsorbents and antimicrobial agents making them an effective agent against all major water pollutants including organic molecules, heavy metal ions and water borne pathogens, respectively. This article presents a comprehensive review on the application of metal oxide/graphene composites in water treatment and their role as photocatalyst, adsorbent and disinfectant in water remediation. Through this review, we discuss the current state of the art in metal oxide/graphene composites for water purification and also provide a comprehensive analysis of the nature of interaction of these composites with various types of pollutants which dictates their photocatalytic, adsorptive and antimicrobial activities. The review concludes with a summary on the role of graphene based materials in removal of pollutants from water and some proposed strategies for designing of highly efficient multifunctional metal oxide/graphene composites for water remediation. A brief perspective on the challenges and new directions in the area is also provided for researchers interested in designing advanced water treatment strategies using graphene based advanced materials.

[a]*Department of Chemistry, School of Natural Sciences, Shiv Nadar University, Gautam Budh Nagar 203207, Uttar Pradesh, India*

[b]*Knowledge Centre for Materials Chemistry (KCMC), Institute for Materials Research and Innovation (IMRI), University of Bolton, BL3 5AB, UK*

[c]*Department of Physics, School of Natural Sciences, Shiv Nadar University, Gautam Budh Nagar 203207, Uttar Pradesh, India. E-mail: susanta.roy@snu.edu.in; Tel: +91-120-2663880*

Ravi Kant Upadhyay did his MSc from Jiwaji University, Gwalior, India. After completing his M.Sc he joined Advance Material and Process Research Institute (AMPRI) as a research intern for two years where he worked on synthesis and characterization of nanomaterials and their environmental applications. He is currently pursuing his PhD at Shiv Nadar University (SNU), India under supervision of Dr Susanta Sinha Roy. He is currently working on synthesis of nanomaterials and their application in water treatment by exploring photocatalysis and adsorption phenomenon.

Dr Navneet Soin received his PhD in 2012, from the University of Ulster, under the direction of Professor James McLaughlin, OBE, where he worked on the microwave plasma synthesis of vertically aligned few layered graphene nanoflakes and their applications in electrochemical energy generation and storage. He is currently a post-doctoral research fellow at the Knowledge Centre for Materials Chemistry (KCMC), University of Bolton where he is working on polymeric materials and structures based energy harvesting. His scientific interests focus on synthesis of carbon nanomaterials for field emission, electrochemical clean energy generation, storage and continuous production of piezoelectric polymeric materials.

1. Introduction

In spite of extensive research in inorganic materials, carbon based materials are increasing in popularity with the scientific communities for exploring various size dependent phenomenon in different research areas, thanks to their simplicity, environmentally benign nature and mass scale availability. Path breaking discoveries of sp^2 hybridised carbon derivatives such as C$_{60}$: buckministerfullerene,[1] carbon nanotubes[2] and graphene[3] at pivotal moments in time have ensured that the research has forayed into new directions and pathways. In the family of carbon nanomaterials, graphene seems to be the one with the most potential due to its outstanding physical, chemical and electronic properties. Graphene, is a two dimensional material having single layer of sp^2 network of carbon atoms, is considered as the thinnest and hardest material known so far.[4–6] The first reported synthesis of the proclaimed "miracle material" by Novoselov *et al.*[3] in 2004 garnered immense interest among researchers resulting in an inundation of studies devoted to various aspects of graphene in last few years. Graphene inherently displays a large number of intriguing and peculiar properties such as high room temperature charge carrier mobility ($\sim$100 000 cm^2 V^{-1} s^{-1}),[7] theoretically large surface area ($\sim$2630 m^2 g^{-1}),[8] optical transparency,[9] excellent mechanical strength (2.4 $\pm$ 0.4 TPa),[10] high thermal conductivity ($\sim$2000 to 5000 W m K^{-1})[11,12] and capacity of sustaining large electrical current density (10^8 A cm^{-2})[13] *etc.* These unique properties endowed within graphene make it an enticing material for variety of applications such as in solar cells,[14–16] liquid crystal devices[17] capacitors,[8,18] batteries,[19–21] sensors[22–24] and water treatment[25–32] among many other applications.

While incredible strides in science and technology have indeed raised the quality and standard of the human life and health, it has nevertheless brought about a multitude of problems as well. Among them, water pollution and contamination is one of the biggest and the most alarming problems that demands formidable and effective solutions. Particularly in developing countries the situation is worrisome and the non-availability of *economical* water treatment techniques further aggravates the situation.[33,34] Although huge initiatives are already underway to tackle this problem, further and highly rigorous research dedicated to this issue is still required. Historically carbon based materials, especially high surface area activated carbons have been widely explored for water purification.[35,36] Going by the surface area premise, graphene, which theoretically exhibits nearly twice the surface area of well developed activated carbon can provide a much better alternative.[37] Recently, graphene and its derivatives have emerged as a key material for designing experimental water treatment strategies owing to their excellent aforementioned physical, chemical and electronic properties. This article aims to present a comprehensive review on application and utility of metal oxide/graphene nanocomposites for removal of three major water pollutants namely, organic molecules, heavy metals and waterborne pathogens (Fig. 1).

The initial demonstration by Fujishima and Honda, of electrochemical photolysis of water by TiO$_2$ (ref. 38) led to an incredible amount of research into the investigation of photocatalytic activity of various metal oxides. Apart from photolysis of water, metal oxides have also been employed as a photocatalyst for the degradation of various water pollutants and have shown promising results.[39,40] However, in spite of having several promising features, the devices based on these metal oxide constituents are still not able to compete with the traditional water treatment practices and techniques such as reverse osmosis and filtration. This failure can be attributed to some of the shortcomings associated with these metal oxides.

Dr Susanta Sinha Roy, (Associate Professor, Shiv Nadar University, India) obtained his M.Sc in Physics from Calcutta University and PhD in science from Jadavpur University, India. He has 14 years research work experience in UK, Germany and Canada. His carbon materials and microfluidics research laboratory at the Shiv Nadar University is active in the field of nano-materials, nano-structured surfaces, MEMS and developing new approaches/concepts suitable for microfluidic sensors, water and energy related applications. He has published over 70 research papers in the peer reviewed journals of international repute, presented over 60 conference papers (h-index = 17). Dr Roy has teaching experience in courses of materials science and engineering, thermal physics, bio-medical engineering and molecular spectroscopy.

Fig. 1   Three major types of pollutants present in water.

Especially, the wide band gap of metal oxides which limits their activity to UV region only and the possibility of charge carrier recombination which shorten the life time of the active species which are responsible for the degradation of pollutants. Several strategies such as doping, surface modification and amalgamation of metal oxides with electron scavenging agents backed by theoretical density functional theory simulations have been tried to solve these issues.[41–45] Out of the aforementioned practices to improve the photocatalytic efficiency of the metal oxides, combination of metal oxides with electron scavenging agents has been one the most popular and exploited approach to attenuate the effect of the large band gap and electron hole recombination on the photocatalytic performance. A variety of electron scavenging agents such as metals,[42,43] carbonaceous materials[44,45] and polymers[46] have been combined with metal oxide nanoparticles. Carbonaceous molecules such as carbon nanotubes, fullerenes and graphene are the preferred candidates of choice as electron acceptor molecule owing to their inherent advantages such as low cost, innocuous nature, ease of availability and processing. Out of these carbonaceous molecules, graphene derivatives have acquired great interest as a support material for the formation of nanocomposites with metal oxide because of availability of a large number of economical and facile synthesis approaches and possibility of surface which have been developed over the years *via* the work on other forms of carbon such as nanotubes and fullerenes. Fig. 2 illustrates the mechanism involved in photocatalytic activity of graphene/metal oxide composite.

Adsorption is one of the most exploited phenomenon for the desalination of water. As compared to other water treatment practices, it offers several advantages such as the ease of performance, no harmful generation of by-products during the course of treatment and above all, it can remove nearly all types of pollutants from waste water.[47] Especially, for the removal of toxic heavy metal ions adsorption is the preferred approach, as the metal ions cannot be degraded by photo-catalysis or any other chemical reaction. The two-dimensional atomic chicken-wire structure of graphene[48] can serve as a mesh containing pores of fine size for removal of pollutants from water. Also, as a prerequisite, graphene exhibits a much higher theoretical surface area than activated carbon and thus can act as an efficient adsorbent. In addition to unprecedented surface area, graphene and its oxide derivative, graphene oxide, also provides freedom of introduction of functionalities[49] which can favour selective adsorption of pollutants. Graphene oxide is highly acidic in nature therefore can readily adsorb basic molecules and cations. Until now, graphene has been explored as an adsorbent for the removal of various dyes,[50–52] heavy metal ions[53–55] and other aromatic pollutants.[56–58] Besides the application of pristine graphene as an adsorbent, graphene modified with surfactant,[59] nanomaterials,[60–63] polymers[64,65] and biomolecules[66] have also been explored as adsorbents and are found to be exhibit excellent adsorption efficiency. Presence of active groups such as carbonyl, epoxy and hydroxyl groups on the surface of graphene oxide enables it to interact with a wide variety of molecules and thus can undergo surface modification. Moreover, these entangled active groups of graphene oxide can also bind to the heavy metal ions present in the solution *via* surface complexation so it can also be used to extract ions from solution.[67] Recently, numerous studies devoted to utilization of self assembled metal oxides nanomaterials on graphene and reduced graphene oxide for removal of different water pollutants have been reported. The incorporation of metal oxide nanoparticles on graphene limits their re-stacking and aggregation, thereby enhancing the surface area of the composite.[68,69] At the same time, *in situ* growth of metal oxide nanoparticles on graphene results in less agglomeration among particles as graphene sheets acts as building blocks for the nanoparticles growth and keeps them in dispersed form. Furthermore, the functional groups and defect sites of graphene act as the nucleation and growth sites for nanoparticles. The combination of graphene with the metal oxide extends the life time of the adsorbent material by acting as support material which inhibits leaching of fine metal oxides particles into the treated water.
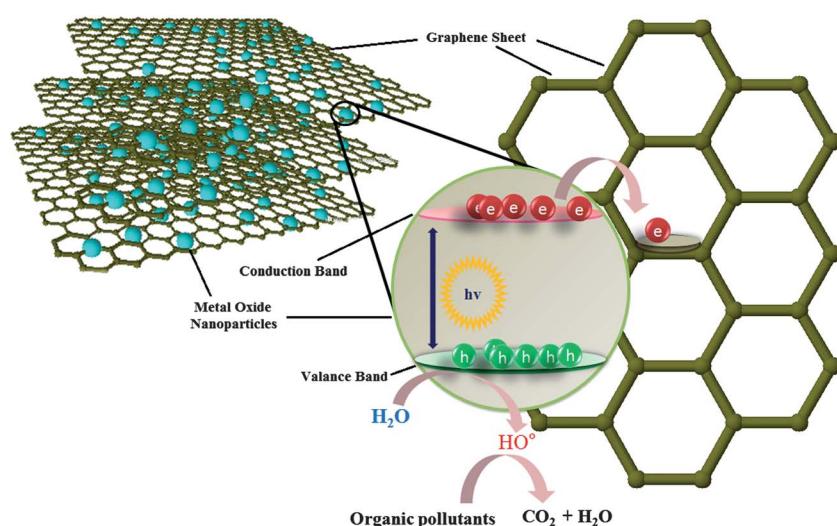
Fig. 2 Electron transfer from conduction band of metal oxide to graphene through percolation mechanism.
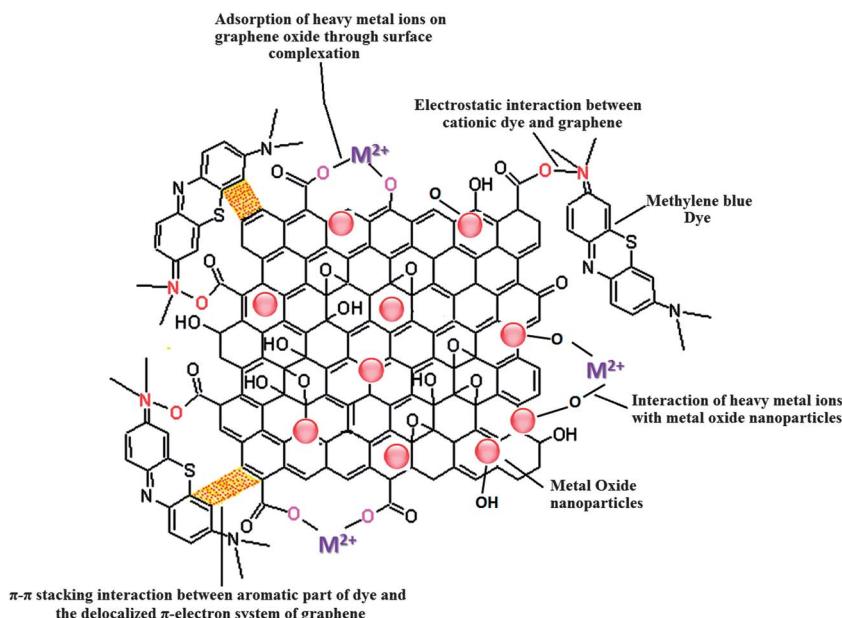
Fig. 3 Different types of interactions in involved in the adsorption of pollutants on metal oxide/graphene oxide.

Also, the amalgamation of graphene with metal oxide renders mechanical strength to the composite and increases the robustness of the adsorbent. Modes of interaction of graphene/metal oxide composite with different type of pollutants are shown in Fig. 3.

Recently, the research on antimicrobial activity of nano-materials has gained pace and several efforts are being made to search the possibility of real life applications for this remarkable property of nanomaterials. Again, graphene has emerged as one of the most promising materials for application as antimicrobial materials.[70–73] Other than the presence of organic pollutants and heavy metals, the presence of waterborne pathogens in water is also deleterious for human health which needs to be addressed. For this, graphene derived materials having antimicrobial activity can be employed for remediation and sterilization of water. Further coupling of graphene with metal oxide can greatly enhance its antimicrobial activity as metal oxides can contribute to the antimicrobial activity of graphene either by producing active oxidative species which destructs the cell or by promoting the adherence of the more cells to the graphene by increasing the surface area of the graphene. Other than this, few metal oxides (Fe_3O_4 and TiO_2) themselves exhibit antimicrobial activity, so a composite of these metal oxides with graphene can exhibit excellent antimicrobial activity due to synergistic effects.

This review aims of extending information related to the utilization of metal oxide/graphene composite for water remediation and evaluation of their activity against different types of waterborne pollutants. The work also discusses the possible mechanisms involved in degradation of different pollutants by metal oxide/graphene composite. In light of the increasing concerns related to issue of water pollution, the search of new and more effective water treatment strategies is highly desirable and we believe that this review can provide a comprehensive

current state-of-the-art in the area and will prove helpful in designing new water treatment strategies by building upon the current strategies.

2. Graphene/metal oxide nanocomposites as photocatalyst for waste water treatment

Recently, a large number of studies have been published on the application of graphene/metal oxide nanocomposites as photocatalysts and for water purification owing to its exceptional properties exhibited by the composites such as higher adsorptivity, conductivity, tuneable optical behaviour, stability and longevity. Reduced graphene oxide (a derivative of graphene oxide) has been combined with variety of metal oxides such as TiO_2,[74] ZnO,[75] Cu_2O,[76] $ZnFe_2O_4$,[77] $CuFe_2O_4$[78] and Bi_2WO_6[79] and found to be an excellent photocatalyst for the degradation of synthetic dyes. Other than limiting the electron hole recombination, graphene oxide derivatives also prevent the corrosion and leaching of the metal oxide nanoparticles in to the water thereby enhancing the longevity of the photocatalyst. Also, the formation of $\pi–\pi$ stacking between aromatic rings of graphene and organic pollutants also facilitates the adsorption of pollutants on the photocatalyst thereby enhancing the quenching of pollutants.[80] In the following sections we discuss the synthesis routes, mechanisms and applications of graphene/metal oxide composites, especially in the area of photocatalysis.

2.1. Graphene/TiO₂ composite as photocatalyst

TiO_2 is one of the most "*popular*" and widely used photocatalyst and has been widely explored for water purification. The advantages of TiO_2 over other metal oxide such as innocuous

Table 1 Different TiO$_2$/graphene composites used for the photodegradation of pollutants

Graphene composite	Particle size of TiO$_2$	Graphene content	Targeted pollutant	Ref.
TiO$_2$/GR	8.6–9.1 nm	3 wt%	Methylene blue	110
TiO$_2$/GR–Ag$_2$Se	15 nm	—	Rhodamine B	111
TiO$_2$ nanotubes/GR	320 nm length, 90 nm pore diameter	—	2,4-Dichlorophenoxyacetic acid	43
Pt–GO–TiO$_2$/GR	30 nm	0.5 wt%	Dodecylbenzenesulfonate (DBS)	42
TiO$_2$–GO and TiO$_2$–G	5–15 nm	90%	Methylene blue	112
Nd/TiO$_2$/GR	8–12 nm		Methyl orange	109
TiO$_2$/GR	—	—	Methylene blue	113
TiO$_2$/GR	4–5 nm	75 wt%	Methylene blue	114
TiO$_2$ nanowires/GR	<20 nm diameter	25.6% carbon content	17β-Estradiol (E2)	115
TiO$_2$/GR	4 nm	47.31 wt%	Methylene blue	116
TiO$_2$/GO	—	10 mg	Methylene blue	117
G-N/TiO$_2$-x/GR	—	2 wt%	Benzoic acid	97
TiO$_2$/RGO	20 nm	1 wt%	Rhodamine B (RhB) and acid orange II (AO-II)	118
TiO$_2$/GR	25 nm	3 wt%	Methylene blue	94
TiO$_2$/GR	—	10 wt%	Methyl orange	119
La/TiO$_2$/GR	8–12 nm	—	Methylene blue	120
TiO$_2$/GR	Diameter 4 nm length 25 nm	5 wt%	Methylene blue	80
TiO$_2$/GR	30–40 nm	Graphene : TiO$_2$ = 1 : 3 mass ratio	Methylene blue	121
TiO$_2$/RGO	—	GO and P25 weight ratio 1 : 40	Rhodamine B	122
TiO$_2$/GO	57 nm	3.3 wt%	Diphenhydramine (DP)methyl orange (MO)	123
Fe–TiO$_2$/GR	8.0–12.0 nm	—	Methyl orange	41
TiO$_2$/GO	50 nm thickness	10 wt%	Methylene blue	124
TiO$_2$–CeO$_2$/GR	25 nm	5 wt%	Reactive red 195 and 2,4-dichlorophenoxyacetic acid	125
G-Au–TiO$_2$/GR	100–200 nm	—	Methylene blue	108
TiO$_2$/GO	20–40 nm	4.6 wt%	Methyl orange	126
TiO$_2$/GR	—	5%	Cr(VI) reduction	127
CdSe–TiO$_2$/GR	<25 nm	34.22 wt% carbon	Methyl orange (MO) and Rhodamine B (RhB)	96
TiO$_2$/GO	30 nm	10 wt%	Methylene blue	128
TiO$_2$/GR	<10 nm	8.5% wt ratio	Rhodamine B	129
TiO$_2$/GO		Weight ratio of GO to TiO$_2$-1.5	Methyl orange	130
TiO$_2$/GO	10 nm	0.03 mg GO	Methylene blue	92
TiO$_2$/GR	10–30 nm	3 wt%	Methylene blue	131
TiO$_2$/GR	10–15 nm	10.8% carbon content	Rhodamine B	132
ZnO–TiO$_2$/RGO	—	10 wt% TiO$_2$	Reduction of Cr(VI)	133
SiO$_2$–TiO$_2$/GR	5 nm pore diameter	1%	Atrazine	88
Titanate/GR	7–9 nm diameter	—	Phenol	134
TiO$_2$ nanotubes/GR	~9 nm	5 wt%	Rhodamine-B	135
TiO$_2$/GO	4–5 nm	3.3–4.0 wt%	Diphenhydramine (DP) and methyl orange (MO)	136
TiO$_2$/GR	7–8 nm	0.05 wt%	Acetone	93
TiO$_2$/GO	15 nm	~10%	Rhodamine B	95
TiO$_2$/GR	18 nm	—	Rhodamine B	137
TiO$_2$/GO	10 nm	Weight ratio of GO/TiO$_2$ = 3 : 2	Methyl orange	138
TiO$_2$/GO	6–9 nm	1 wt%	Methylene blue	139
TiO$_2$/GR	5 nm pore diameter	1%	Rhodamine B and norfloxacin	140
TiO$_2$/GR	20–200 nm	—	Methylene blue	141
TiO$_2$/GR	12.3–41.0 nm	—	Butane	142
TiO$_2$/GR films	100 nm thickness	3 wt%	Methylene blue	143
TiO$_2$/MCM-41/GR	—	0.15 wt%	2-Propanol	144
TiO$_2$/RGO	12–16 nm	2.0 wt%	Rhodamine B	145
TiO$_2$/RGO	9 nm	10%	Malachite green	146
TiO$_2$ (P25)/GR		1 wt%	Methylene blue	91
TiO$_2$/RGO	18 nm	15%	Rhodamine B	74

nature, cheap and chemically stable makes it superior.[81,82] Owing to the 3.2 ev[83] band gap of TiO$_2$ its photocatalytic activity is restricted to the ultraviolet region only and is the single biggest contentious issue with it. Several strategies such as doping,[84,85] introduction of defects[86,87] and combination of it with electron acceptor materials[88–91] have been tried to reduce the band gap to make it active in visible region. Out of these strategies combination with electron acceptor materials is one of the most frequently explored. Graphene too has also been explored as electron acceptor molecule for making composite with TiO$_2$ and some of the TiO$_2$/graphene composites reported in different studies are tabulated in Table 1. Coupling of TiO$_2$ with graphene has been shown to enhance the photocatalytic performance of the composite. The combination of metal oxide nanoparticles with graphene derivatives leads to the reduction in the band gap of the metal oxide *via* energy favoured hybridisation of O2p and C2p atomic orbitals which results in formation of new valance band.[88] Now, for an efficient catalyst–support interaction to occur, the amount of metal oxide loading to the graphene support material needs to be carefully tuned. In fact, the percentage of the graphene content plays a key role in deciding the photocatalytic activity of the composite and variation in the amount of graphene component exerts a marked effect on performance of resulting photocatalyst. In general increase in the graphene content in composite improves photocatalytic activity but increasing the graphene content beyond a certain threshold limit can lead to a reduction in the photocatalytic activity through enhancing absorption and scattering of photons by excess carbon content present in the composite.[92] Wang *et al.* studied the effect of graphene loading on activity of TiO$_2$–graphene composites and optimized the threshold weight percent of graphene (0.05 wt%) for obtaining maximum photocatalytic activity.[93] Photocatalytic activity of hybrid material highly depends on the interface between TiO$_2$ and graphene, an intense coupling between TiO$_2$ and graphene facilitates charge separation and so retards recombination. The *in situ* growth of TiO$_2$ on graphene or graphene on TiO$_2$ can provide much more efficient hybrid photocatalysts. Wang *et al.*[94] have developed a method for the *in situ* preparation of graphene like carbon structures on TiO$_2$ which show nearly 2.5 times enhanced photodegradation of methylene blue dye when compared to pristine Degaussa P25 TiO$_2$. Liang *et al.*[95] have reported on the growth of uniform growth of TiO$_2$ nanocrystals directly on graphene oxide substrate (Fig. 4) *via* hydrolysis coupled hydrothermal treatment. The as prepared GO–TiO$_2$ hybrids showed a three-fold photocatalytic activity for the degradation of Rhodamine B dye as compared to P25 TiO$_2$. This enhancement was attributed to an improved electronic coupling between graphene oxide and TiO$_2$ nanocrystals and higher surface area of the hybrid material.

In a recent study, a composite of CdSe decorated TiO$_2$ on graphene has been shown to achieve improved photocatalytic efficiency, *via* the coupling of CdSe with TiO$_2$ which improves the photocatalytic activity of TiO$_2$ in visible region.[96] Khalid *et al.*[41] have prepared the composite of Fe doped TiO$_2$ with graphene and tested its photocatalytic activity for degradation of a synthetic dye, methyl orange. A tenfold increase in the
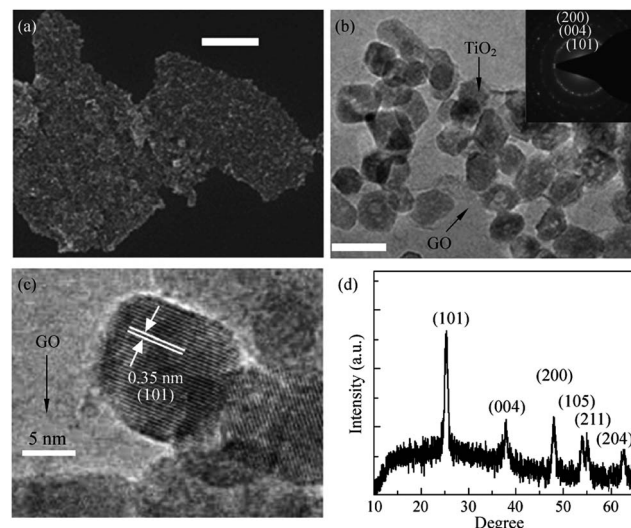
Fig. 4 (a) SEM image, (b) low magnification, and (c) high magnification TEM images of TiO$_2$ nanocrystals grown on GO sheets. The scale bar is 400 nm for the SEM image in (a) and 20 nm for the TEM image in (b). (d) An XRD pattern of the graphene/TiO$_2$ nanocrystals hybrid. Reprinted with permission from ref. 95 Copyright 2010, Springer Science + Business Media.

photocatalytic activity was observed for the composite over pure TiO$_2$ which was attributed to the synergistic effect of improved adsorptivity of dyes, enhanced visible light absorption and reduced charge carrier recombination. In an another study, Min *et al.*[97] successfully synthesized composite of N doped TiO$_2$ with graphene and investigated its photocatalytic activity for degradation of benzoic acid. The nitrogen doped TiO$_2$ graphene composites showed enhanced photocatalytic activity as compared to pristine TiO$_2$ graphene composite which was then ascribed to the enhanced response of N–TiO$_2$/graphene composite in the visible region.

In several reports, photocurrent measurements were performed to probe the role of graphene oxide in retarding the charge recombination. A significant increase in the photocurrent for TiO$_2$/RGO composite as compared to bare TiO$_2$ was observed, which elucidates the involvement of the graphene oxide in the charge transport. Shi *et al.*[98] observed a six times higher photocurrent generation in the case of TiO$_2$/RGO composites, as compared to bare TiO$_2$. This enhancement in the photocurrent was ascribed to the immediate capture of photoexcited electrons by the reduced graphene oxide from TiO$_2$ and their subsequent quick transportation to the external circuit. Photocurrent response generated by bare TiO$_2$ exhibited spikes, which was ascribed to the sudden rise in photocurrent due to accumulation of electrons in the conduction band which occurs during the initial photo-irradiation time, followed by a rapid electron–hole recombination which caused photocurrent decay. In fact, for TiO$_2$-reduced graphene oxide samples, these spikes were absent, owing to the efficient transfer of the electrons from conduction band to the external circuit which shows that the coupling of TiO$_2$ with reduced graphene oxide not only enhances the photochemical response of the TiO$_2$ but also improve the quality of photocurrent.
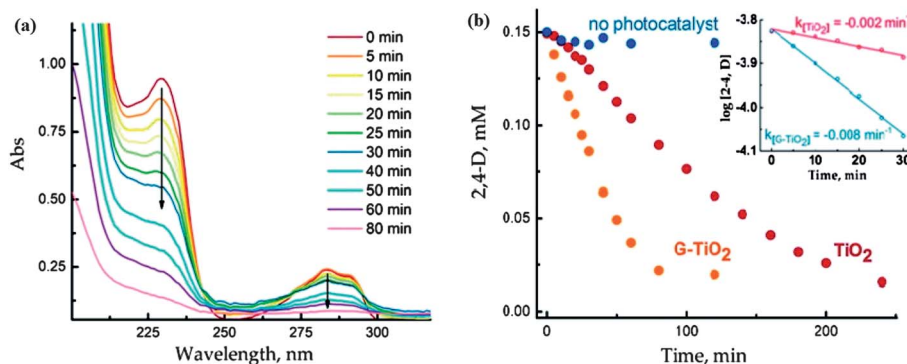
Fig. 5 (A) Absorption spectra of aqueous solution (O_2 saturated) of 0.15 mM 2, 4-D recorded following of aqueous solution (O_2 saturated) of 0.15 mM 2, 4-D recorded following UV-excitation of RGO−TiO_2 film. (B) The decrease in 2,4-D concentration following the UV photolysis with TiO_2 and RGO−TiO_2 films. The blank experiments recorded in the absence of photocatalyst are also shown. Inset shows the pseudo-first-order fit of 2,4-D decay during initial 30 min of UV excitation. Reprinted with permission from ref. 102, Copyright (2010) American Chemical Society.

The photoactivity of TiO_2 reduced graphene composites also depends on the preparation route followed. For instance, the use of strong reducing agent for the reduction of graphene oxide to graphene may leave impurities in the final product or can result in the restacking of individual graphitic layers[99–101] which can impede the photoactivity of the composite. Ng et al.[102] did a comparative study between TiO_2/RGO obtained through photocatalytic reduction of graphene oxide and TiO_2/RGO prepared using hydrazine as reducing agent in terms of photocurrent generation by these two composites and calculated the IPCE (incident photon to photocurrent efficiency) value for each one. The maximum IPCE value for photocatalytically reduced RGO and hydrazine reduced RGO was 13.9% and 11.4%, respectively which revealed the superior performance of photocatalytically reduced RGO. The authors also investigated the photocatalytic activity of pristine TiO_2 and TiO_2/RGO for degradation of 2,4-dichlorophenoxyacetic acid and observed a four-fold enhancement in the rate of photocatalytic degradation by TiO_2 hybridized with RGO as compared to pristine TiO_2. Enhanced photocatalytic activity of TiO_2/RGO was attributed to π−π stacking mediated adsorption of 2,4-dichlorophenoxyacetic acid on to the TiO_2/RGO surface which facilitated the interaction of photogenerated active species and 2,4-dichlorophenoxyacetic acid at TiO_2/RGO interface. Fig. 5(a) shows UV-Vis absorption spectra of 2,4-dichlorophenoxyacetic acid recorded at different time intervals during its photocatalytic decomposition at UV-irradiated RGO−TiO_2 film and Fig. 5(b) shows the graph between absolute concentrations of 2,4-dichlorophenoxyacetic acid vs. time showing the superior photo-catalytic performance of RGO−TiO_2. Obviously, reaction conditions such as reaction temperature and time also exhibit a pronounced effect on the photocatalytic activity of the composite. Photocatalytic activity of the composite can be improved by judicial optimization of reaction parameters. Zhang and co-workers[103] studied the effect of hydrothermal reaction time on the photocatalytic activity of the TiO_2/graphene composite and observed a marked increase in the photocatalytic activity of the TiO_2/graphene on extending reaction time which was the outcome of better synergistic interaction between TiO_2 and graphene sheet.

The photocatalytic activity of the TiO_2/GR is essentially exhibits the same mechanism as other nanocarbons such as carbon nanotubes and fullerenes. Nevertheless, graphene itself exhibits some tremendous properties such as higher surface area, higher conductivity and flexibility, which makes this 2D carbon form superior as a support material for fabrication of composite. One of the major advantages which graphene endows is its ease of fabrication as compared to other carbonaceous molecules belonging to the same family. There are large numbers of available methods, within the bottom up and top down approaches which can be employed for the facile synthesis of graphene. Converting graphite to graphene oxide using Hummer's method followed by reduction of graphene oxide using a suitable reducing agent to yield graphene is one of the most frequent approaches tried by researchers. Fig. 6 shows TEM images of graphene sheets grown by chemical reduction of graphene oxide prepared using modified Hummers method.[104] However, there are only a few reports available in the literature which have proclaimed higher photocatalytic efficiency for composite having graphene as support as compared to carbon nanotubes.[91] But there are few studies which denies superiority
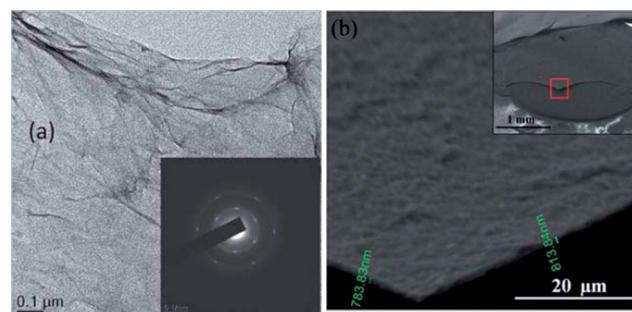

Fig. 6 (a) Low magnification TEM image of GO flakes with selected area electron diffraction (SAED) in the inset. (b) Cross-sectional high magnification SEM image of GO films at the cut highlighted in the inset. The thickness of the film is about 800 nm. Inset shows the image of GO films drop dried on GCE. The film is spread uniformly without localized aggregation. It was broken using tweezers and a certain portion of it was removed, thereby exposing the underlying GCE. Reproduced with permission from ref. 104.

of graphene over carbon nanotubes in terms of enhancing photo-catalytic activity of metal oxides and suggest that both of the carbon analogues affects the photocatalytic activity of metal oxide to a similar extent. Yang et al.[105] synthesized TiO$_2$ composite with graphene, carbon nanotubes and C$_{60}$ and examined the photocatalytic activity of all three composites for the selective oxidation of benzyl alcohol to benzyl aldehyde and did not observe any significant differences in the photocatalytic activity of all the three composite, which shows that the carbon analogues have similar activity and follow similar oxidation mechanism. Zhang and co-workers[106] have performed a detailed study to investigate the proposed superiority of graphene over carbon nanotubes in terms of improving photocatalytic activity of TiO$_2$ and found that method used for TiO$_2$/graphene composite preparation plays a key role in deciding its photocatalytic activity, method which facilitates more intimate interfacial interaction among TiO$_2$ and graphene sheets gives product with enhanced photocatalytic activity. The enhanced photocatlytic response of photocatalyst on these carbonaceous materials originates from essentially the same underlying principles of enhanced adsorptivity, expanded light absorption range and suppression of electron hole recombination. Thus, the role of microstructure and dimensionality of the support material needs further investigation vis-à-vis further comparative experiments using various carbon analogues along with DFT analysis. Recently Geng et al.[107] used density functional theory (DFT) to probe enhancement in the photocatalytic activity of TiO$_2$ upon coupling with graphene. TiO$_2$ clusters were anchored on three representative structures pristine graphene (P-G), graphene with monovacancy (V-G) and graphene with epoxy (O-G). Geometric configurations and binding energy results revealed that binding of TiO$_2$ with V-G and O-G is more stable compare to the P-G and the minimum iso-surface values on the electronic total charge density plots follow following order TiO$_2$–P-G < TiO$_2$–V-G < TiO$_2$–O-G which reflects increase in covalent interaction from TiO$_2$–P-G to TiO$_2$–O-G. On the basis of analysis of calculation results, following two reasons were given for the enhanced photocatalytic activity of TiO$_2$ on combining with graphene; firstly the reduction in the electron and hole recombination due to separation of valance bands (VBs) and conduction band maximum (CBM) by location at cluster and graphene sheet and secondly, the valance band maximum (VBM) contributed from C-2p is lower than for Ti-3d which decrease the excitation energy in the visible light region. Further, surface modification of TiO$_2$ graphene composite with metal ions such as Ag,[43] Pt,[42] Au,[108] Fe,[41] Nd[109] etc. can also improve photocatalytic activity of the composite. These metals have been shown to prolong the life time of charge carriers by trapping excited electrons so as to further diminish the recombination of charge carriers.

2.2. Photocatalytic activity of graphene composite with metal oxide other than TiO$_2$

Apart from TiO$_2$, large numbers of metal oxides and complex oxides such as ZnO,[147–150] WO$_3$,[151] CuO,[152] Cu$_2$O,[153] Mn$_3$O$_4$,[154] Mn$_2$O$_3$,[155] SnO$_2$,[156] Bi$_2$WO$_6$,[79] ZnWO$_4$,[157] Bi$_2$MoO$_6$,[158] BiVO$_4$,[159]

BaCrO$_4$[160] and CoFeO$_4$[161] have also been tried in combination with graphene to serve as photocatalyst. The particle size, graphene content and targeted pollutants for different metal oxide/graphene composites have been summarized in the Table 2.

In some cases, composites of graphene with metal oxide other than TiO$_2$ have shown higher photocatalytic performance when compared to TiO$_2$/graphene composite.[162,163] Wang et al.[164] have demonstrated that a combination of SnO$_2$ with graphene improved the photo-catalytic activity of the SnO$_2$ for the degradation of the pendimethalin, which was attributed to the facile transfer of electrons from the excited pendimethalin to SnO$_2$. A larger potential difference between pendimethalin molecule and SnO$_2$ makes the electron transfer process thermodynamically more favourable for SnO$_2$, as compared to other semiconductors (TiO$_2$ and ZnO). The degradation rate constant for the SnO$_2$/graphene composite was observed to be higher as compared to the other semiconductor composite such as P25–graphene, TiO$_2$–graphene and ZnO–graphene under visible light excitation. Xu et al.[149] have performed a detailed study to probe the possible mechanism involved in the photocatalytic activity of ZnO/graphene composite and suggested that the formation of active oxidative species such as O$_2$$^{•-}$, $^•$OH and holes are responsible for the photo-degradation of the methylene blue. It was found that direct hole oxidation and O$_2$$^{•-}$ oxidation are the predominant reactions involved in the photocatalytic process. Enhanced photo-catalytic activity of the graphene hybridized ZnO compare to the mechanically mixed ZnO and graphene revealed that the extent of electronic interaction between the ZnO and graphene governs the photocatalytic activity of the composite. A 3.5 times higher photocurrent generation was observed in the case of ZnO/graphene electrode compare to ZnO electrode which can be attributed to the reduced electron hole recombination. A further positive shift in flat-band potential, obtained from the Mott–Sckottky (MS) plots for ZnO/graphene (−0.29 V) as compared to ZnO (−0.36 V) and lower value of slope of the linear region for ZnO/graphene composite confirmed higher donor density. In order to understand effect of interface structure on the properties of the ZnO/graphene composites, Geng et al.[165] performed DFT calculations for graphene on ZnO layers and ZnO slabs with Zinc and oxygen terminations. It was found that the nature of interaction between ZnO layers and graphene sheet are weak and do not affect electronic properties of the graphene significantly. On the other hand graphene on thick ZnO slabs with polarized surfaces exhibited larger charge transfers and stronger binding energies. The change of termination element of graphene on thick ZnO surface also changed the conductivity of the composite. Graphene on thick ZnO surface with Zn termination shown n-type conductivity and increased work function however graphene on ZnO surface with oxygen termination displayed p-type conductivity and lower work function.

The extent of defects in the crystal structure of the metal oxide component of the composite also influences the photocatalytic performance of the composite. Chen and co-workers[166] investigated the effects of zinc and oxygen vacancies in the ZnO lattice on the photo-catalytic activity of the ZnO/RGO composite. The presence of zinc and oxygen vacancies improves

the

Table 2 Composite of metal oxides other than TiO_2 with graphene and graphene oxide used as photocatalyst for the degradation of pollutants

Graphene composite	Particle size of metal oxide	Graphene content	Targeted pollutant	Ref.
ZnO/GR	5 nm	2.5%	Methylene blue	75
ZnO nanorods/RGO	200 nm in diameter 600 nm in length	Mass ratios of GO to $Zn(NO_3)_2 \cdot 6H_2O = 1:2$	Methylene blue	148
ZnO/GR	10–20 nm	2 wt%	Methylene blue	149
ZnO/GO	0.5–1 μm	—	Methylene blue	172
ZnO/RGO	70 nm	—	Methylene blue	173
ZnO/GR	30 nm–150 nm	2%	Methylene blue	174
Ag_3PO_4/GR	100–500 nm	15 wt%	Methyl orange	175
Mn_2O_3/GR	8–10 nm	—	Methylene blue, eosin and Rhodamine B	155
Cu_2O/GR	21 ± 3 nm	—	Methylene blue	153
ZnO@ZnS/graphene	250–500 nm	80 mg	Methyl orange	176
Bi_2WO_6/GR	—	Graphitic carbon 78%	Rhodamine B	177
$CoFe_2O_4$/GR	5.53 nm	5 wt%	Methylene blue	161
		40%	Methylene blue (MB), Rhodamine B (RhB), methyl orange (MO), active black BL-G and active red RGB	
$BiVO_4$/RGO	150 nm	2 wt%	Ciprofloxacin	159
$BiVO_4$/GR	88 nm	—	Methylene blue	178
Bi_2WO_6/GR	—	1.5 wt%	Methylene blue	179
GO–Ag/Ag_3PO_4	150 nm	—	Methyl orange	180
ZnO/GR	90–120 nm	—	Malachite green	181
γ-Bi_2MoO_6/GR	4.5 nm	1.0 wt%	Methylene blue	182
BiOI/GO	700 nm length and diameter 65 nm	~0.5 wt \%	Methyl orange	183
WO_3 nanorods/Gr	7–10 nm	3.5 wt%	Rhodamine B	151
Bi_2MoO_6/GR	200–500 nm	2.5%	Brilliant red dye X-3B	184
CuO/GR	—	30 mg	Methylene blue	152
BiOBr/GR	—	~6 wt%	Sulforhodamine 640 dye	185
ZnO/RGO	—	—	Methylene blue	186
$ZnFe_2O_4$/GR	7–10 nm	20%	Methylene blue	77
$ZnWO_4$ nanorods/GR	Length ~1 μm diameter ~30 nm	0.2 wt%	Methylene blue	157
BiOBr/GR	—	Molar ratios of Bi and graphene 100 : 1	Removal of NO	187
Mn_3O_4/RGO	29.2 nm	—	Orange II	154
Ag_3PO_4/GR	250 nm	—	Rhodamine B, methyl orange, methylene blue	188
$Bi_5Nb_3O_{15}$/GR	—	3%	Rhodamine B	189
WO_3 nanorods/GR	—	—	Methyl orange	190
SnO_2/GR	3.4 nm	15 wt%	Rhodamine B	163
ZnO nanorods/GR	Length 50–200 nm, diameter 15–30 nm	2%	Methylene blue	191
ZnO/RGO/carbon nanotube			Methylene blue	192
ZnO/GR sheets	~7 nm	ZnO content 39.8% and 21.5%	Rhodamine 6G	193
$BaCrO_4$/RGO	5 5 nm	2.0 wt%	Methylene blue	160
ZnO/GR	~200 nm	—	Rhodamine B	194
ZnO/GR	100 nm	10 mg	Methylene blue	195

Table 2 (Contd.)

Graphene composite	Particle size of metal oxide	Graphene content	Targeted pollutant	Ref.
ZnO/ZnFe$_2$O$_4$/GO	10–20 nm	4%	Methylene blue	196
ZnO/GO	~20 to 40 nm	—	Crystal violet	197
ZnO/GR	50–500 nm	5%	Methylene blue	198
ZnO/RGO and Ta$_2$O$_5$/RGO	31.8 nm and 63.9 nm	3 wt%	Methylene blue	199
ZnO/RGO	10.7 nm	ZnO loading 11.55 wt%	Rhodamine-B and Methylene blue	200
ZnO/GR	3 μm	—	Methylene blue	201
ZnFe$_2$O$_4$/GR	40 nm	14.9%	p-Chlorophenol	202
La$_2$Ti$_2$O$_7$/GR	—	—	Rhodamine B	203
ZnO/GR	200–500 nm	—	Methylene blue	204
Fe$_2$O$_3$/ZnO/GR	<10 nm	—	Methylene blue	205
ZnFe$_2$O$_4$/GR	200 nm	—	Methylene blue, methyl orange and Rhodamine B	206
Cu$_2$O/SnO$_2$/GR	3–5 nm	—	Pendimethalin	164
Ag$_3$PO$_4$/RGO	5–10 nm	1 wt%	Methylene blue	207
Cu$_2$O/CNTs/rGO	500 nm	—	Methyl orange	208
Cu$_2$O/RGO	100–500 nm	—	Methylene blue	209
Bi$_2$Fe$_4$O$_9$/GR	100–200 nm	6%	Methyl orange	210
CuO/TiO$_2$/GR	~30 to 50 nm	—	Methylene blue	211
InNbO$_4$/GR	100 nm in width and 200 nm in length	—	Methylene blue	170
ZnO/GR	22 ± 6 nm	0.1 wt%	Methylene blue	212
ZnO/GR	6 nm	10 mg	Methylene blue	213
Ag/ZnO/GR	700 nm	—	Methylene blue	214
ZnO/GR	10 nm	—	Rhodamine B	215
ZnO/GR	10–20 nm	1.2 wt%	Methylene blue	216
CuFe$_2$O$_4$/GR	120–150 nm	25 wt%	Methylene blue	78
ZnO–RGO–Au	Diameter and length of ZnO nanorods are 40 and 750 nm	—	Rhodamine 6G	217
W$_{18}$O$_{49}$/GR	2–3 nm	—	Methyl orange	218
Bi$_{25}$FeO$_{40}$–GR	—	—	Methylene blue	219
Bi$_2$WO$_6$/RGO	3–5 nm	—	Rhodamine B methylene blue and phenol	220
BiOBr/GR	Diameter 50–200 nm	1%	Methyl orange	221
α-SnWO$_4$/RGO	7 nm	6 wt%	Methyl orange	222
BiOBr-GR	—	—	Rhodamine B	223
SnO$_2$/GR	3–5 nm	—	Methylene blue	156
Bi$_2$WO$_6$/GR	—	—	Rhodamine B	79
ZnO/GO	100–200 nm	Zn/GO ratio-15%	Methylene blue	162
ZnO nanorods/GR	Width 10–40 nm, length 20–120 nm	1.2–2.0%	Methylene orange	166
ZnO/GR	10–20 nm	—	Rhodamine B	167
ZnO/GR	400–500 nm	3.56%	Methylene blue	168
ZnO/GR	30 nm	ZnO/GR ration 40 : 1	Methylene blue	169

photo-catalytic activity by preventing charge carrier recombination. Zinc vacancies close to the valence band can trap holes and the oxygen vacancies near to the conduction band can trap electrons and this charge separation enhances the life time of the active charges and prevents electron hole recombination. In addition to the defects in the ZnO, the presence of RGO in the composite as partner material further improves the photo-catalytic activity by extracting electrons from the conduction band of the ZnO. Negatively charged ZnO forms a "visionary heterostructure" with positively charged reduced graphene oxide which facilitates the flow of electron from ZnO to RGO.

The excitation of the semiconductors on exposure to radiation, leads to the generation of electron and holes which further reacts with water or oxygen to produce reactive oxidative species (OH and $O_2^{\cdot-}$). While the role of these species in the degradation of the pollutants *via* photocatalysis is well known; the role of $\cdot OH$ and $O_2^{\cdot-}$ in the degradation of dyes is not very well documented. Li and Cao[167] on observing a significant improvement in the photocatalytic activity of ZnO–graphene composite towards Rhodamine-B dye, further investigated the underlying mechanism. It was observed that instead of excitation of the semiconductor ZnO, excitation of Rhodamine-B dye takes place. The excited Rhodamine-B molecules transfer the electron to the conduction band of the semiconductor or graphene and subsequently produce reactive oxygen species which react with dye molecules and cause the degradation of dyes. Furthermore, the excited dye molecules can be oxidized easily which favour the quick degradation of the dye molecules. The graphs for degradation efficiency *vs.* time for photo-degradation of Rhodamine B dye by ZnO/graphene composite on UV and visible irradiation are shown in Fig. 7(a) and (b), respectively, revealing the higher photo-degradation efficiency of composites as compared to ZnO for both UV and visible radiation. Fig. 7(c) demonstrates absorption spectra of Rhodamine B dye irradiated for different time interval in the presence of graphene, ZnO and ZnO/graphene composite. Reduction of area under peak in UV-Vis spectra confirms the degradation of the dye which is highest in the case of ZnO/graphene composite. Fig. 7(d) explains the effect of amount of dye on photo-degradation efficiency of ZnO/graphene. ZnO/graphene composite exhibits 100% filter efficiency for Rhodamine B dye till the critical solution amount reaches to 160 mL g^{-1} afterwards filter efficiency starts decreasing because of penetration of dye molecules. Similarly, Luo *et al.*[168] prepared composite of ZnO hollow spheres with reduced graphene oxide and noticed a 67% improvement in the photo-degradation efficiency of ZnO on combining with RGO compared to the pristine ZnO hollow spheres. The hybridization of graphene with metal oxide not only improves the photocatalytic activity but also enhances the stability and longevity of the photocatalyst by suppressing the photo-corrosion of the metal oxide.[169]

The morphology of the photocatalyst is also an indispensable factor in deciding the photocatalytic activity of the metal oxide. An *et al.*[151] fabricated one-dimensional WO$_3$ composite with graphene and observed a fifty three times enhancement in the photocatalytic activity for WO$_3$ nanorods graphene composite compare to the commercial WO$_3$. Reaction conditions of pH 2 and temperature 180 °C yielded WO$_3$ nanorods with optimum quality and changing pH from 2 to 1 and 3 produced non uniform and larger agglomerated WO$_3$ nanorods
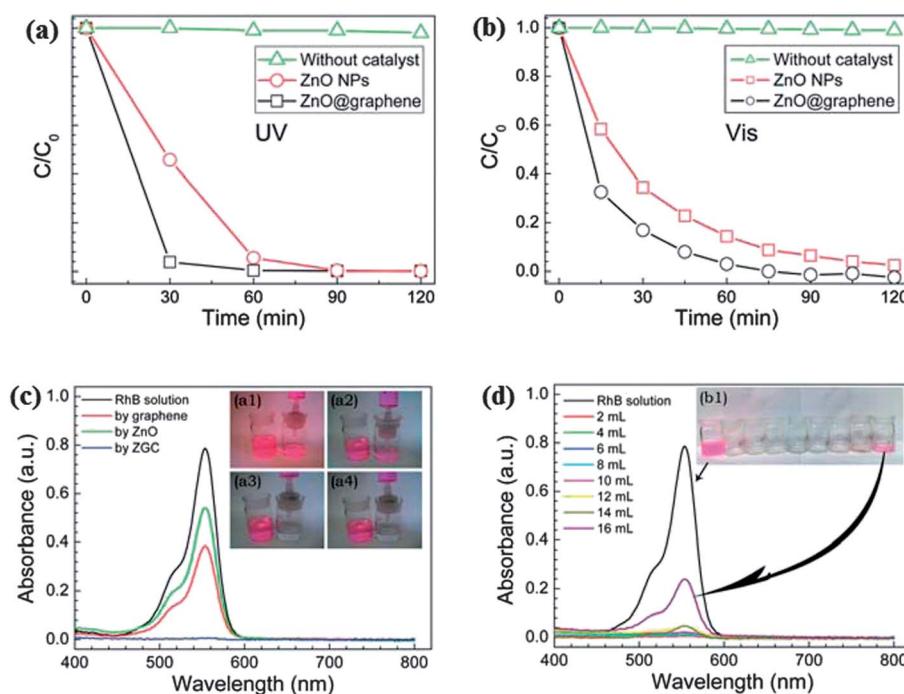

Fig. 7   The photocatalytic degradation of RhB in the presence of ZnO NPs or the ZGC under (a) UV, and (b) visible light irradiation. The UV–visible spectra and images of (c) the original and filtered RhB solutions with graphene (inset a1), commercial ZnO (inset a2), and the ZGC (insets a3 and 4), and (d) the filtrates collected at different amounts of RhB aqueous solution. Reproduced with permission from ref. 167.

respectively and on the other hand a change in reaction temperature from 180 °C to 150 °C and 200 °C, resulted in flowerlike WO_3 structures and corrugation of graphene respectively. Change in pH and temperature not only influenced the morphology but also photocatalytic activity of WO_3/graphene composite with the samples showing reduced photocatalytic activity above and below the optimal conditions.

Other than metal oxides, metallates have also been tried as photocatalyst in combination with graphene. Gao and co-workers[79] have examined the photocatalytic performance of Bi_2WO_6–graphene composite against degradation of organic dye Rhodamine B and observed a three-fold increase in the photocatalytic activity as compared to the pristine Bi_2WO_6, which was attributed to the negative shift in the Fermi level of Bi_2WO_6–graphene and an enhanced transfer of photo-induced electrons at Bi_2WO_6–graphene interface. Bai et al.[157] reported visible photocatalytic activity and enhancement in UV photo-catalytic activity of $ZnWO_4$ by hybridizing it with graphene which was ascribed to the facile charge carrier migration at the $ZnWO_4$/graphene interface. Since, the valence band of $ZnWO_4$ is positioned lower to the highest occupied molecular orbital (HOMO) of the graphene, the photogenerated holes could migrate to the HOMO of graphene from the valence band of the $ZnWO_4$. On the other hand, photogenerated electrons from lowest unoccupied molecular orbital (LUMO) can accumulate to the conduction band of the $ZnWO_4$ as the conduction band of $ZnWO_4$ is located lower to the LUMO orbit of graphene. The authors have made few important observations regarding the generation of active species ($^{\cdot}OH$ and $O_2^{\cdot-}$) during photocatalysis. It was observed that along with the production of these radicals, carbon free radicals are also formed which although, do not directly participate in the degradation reaction but rather prolong the life time of the oxidative species. It was also observed that the reaction pathways for visible and UV exposure are different. While, on visible light irradiation, hydroxyl radical and superoxide radical mediated oxidation pathway dominates; upon the exposure of UV light, holes to become the predominant active species. Zhang et al.[170] achieved 1.87 times higher photocatalytic activity of $InNbO_4$ on combining it with graphene compare to pristine $InNbO_4$ for degradation of methylene blue. Fu et al.[77] studied the photo-catalytic activity of a composite having magnetic complex oxide $ZnFe_2O_4$ and graphene for the degradation of methylene blue in the presence of H_2O_2. Neither H_2O_2 nor $ZnFe_2O_4$ exhibited photo-catalytic activity, nevertheless the coupling of $ZnFe_2O_4$ with graphene enormously enhanced the photo-catalytic activity, which reached to its maximum upon increasing the graphene content up to 20% in the composite. $ZnFe_2O_4$/graphene composite preceded its hydroxyl radical mediated photo-catalytic action *via* two possible mechanisms, first generation of hydroxyl radical by migrated photo-induced electrons from the semiconductor by graphene through a percolation mechanism and secondly, the generation of hydroxyl radical by Fenton reaction.[171] Apart from the excellent photocatalytic activity, $ZnFeO_4$ also acquired magnetic properties which make it quite simple to recover from solution after treatment by using an external magnet.

2.3. Proposed strategies for improving photocatalytic activity of metal oxide/graphene composites on the basis of aforementioned studies

There are certain crucial features and properties of both the components of composite; metal oxide and graphene which must be tuned, to further enhance the photocatalytic activity in conjugation with the resolution of performance impeding issues. Basically, metal oxide is the active constituent which endows the composite with photocatalytic response, and graphene acts as photo-sensitizer and helps in the prevention of charge carrier recombination by collecting photo-excited electrons from the conduction band of the metal oxide. While the role of the support material is crucial, it is the properties of the metal oxides themselves that oversee the optical response of composite. Several features of metal oxides such as band gap, particle size, morphology, extent of defects in crystal lattice and doping with foreign elements are need to be tuned judicially. The shrinking of particle dimensions of metal oxide semi-conductors in to nano-regime enhances the surface area which makes more surface active sites available for the reaction but at the same time it also increases the band gap of semiconductors and thereby increasing the rate of charge carrier recombination. Doping of metal oxides with other elements and introduction of precisely controlled defects in to the crystal lattice of semi-conductors can be helpful in diluting the effect of particle size reduction on optical properties as these defects and dopant can retard charge carriers recombination by trapping them. It has been found that graphene itself can tune the optical characteristics of semiconductors and can promote visible light response of composite thus a more efficient photocatalyst can be designed by taking advantage of synergic effect of doping, defects and graphene on optical properties.

The imperfect and defective structure of graphene is also a major issue with the metal oxide/graphene composite prepared using different approaches. Defects in the structure of graphene exhibit adverse effects on photocatalytic response of the composite so graphene with minimum defects is highly desired for obtaining utmost photo-catalytic performance from composite.[106] Graphene with flawless structure render longer electronic mean free path for electrons and allows them to flow farther from metal oxide/graphene interface making the recombination difficult.[224] Reaction pathway adopted for preparation of metal oxide/graphene composite dictates the structure and property of the graphene so selection of appropriate route and reaction conditions is highly recommended for obtaining graphene with desired properties. Introduction of defects in the metal oxide deliberately in way that it can trap excited electron can also reduce the electron recombination so judicial defect engineering can be an important strategy to improve the photocatalytic activity of the metal oxide/graphene composite. The loading amount of graphene in the composite is also a crucial factor and exerts significant effect on its photo-catalytic activity and needs to be adjusted precisely. Enhancement in graphene content in composite to a certain threshold amount increases the photocatalytic activity but beyond that graphene can impede its photocatalytic activity by preventing

adequate interaction between light and metal oxide. In each case of metal oxide/graphene composites, the optimized graphene contents have been found to be different (Tables 1 and 2) for different pollutant type and application and hence there is need of rational optimization of graphene content in composites prior of its large scale application. There are myriad reports on the importance of interfacial contact between metal oxide and graphene available in the literature. An intimate interfacial contact between metal oxide and graphene favors the transfer of the electrons from the conduction band of the metal oxide to graphene. It has been found that M–O–C bonds between metal oxide and graphene act as channels for migration of electron from metal oxide to graphene. The interfacial contact between metal oxide and graphene can be enhanced by *in situ* growth of the either metal oxide on graphene or graphene on metal oxide, however the former approach is preferred. Metal oxides grown on graphene directly have found to be more efficient compare to the physical mixture of the metal oxides and graphene. The two-dimensional structure of graphene makes it easily accessible for the deposition of metal oxides at the same time availability several active groups on graphene oxide ensures firm binding of metal oxides with graphene sheets. Graphene sheets act as matrix and avoid surface energy derived agglomeration among particles having few nanometer dimensions and in return metal oxide nanoparticles maintains a distance between adjacent graphene sheets and prevent restacking of the sheet.

3. Graphene/metal oxide composites as adsorbents

Theoretically, graphene exhibits a very high surface area (2600 m^2 g^{-1}) which makes it an attractive alternative against the more traditional adsorbents, such as activated and mesoporous carbons. To this effect, graphene and its derivatives have been explored as adsorbents for the removal of pollutants.[28,225–230] The adsorption efficiency of the graphene can be greatly enhanced by making a composite of it with other nanomaterials. As discussed earlier, nanomaterials posses a higher surface to volume ratio and hence a composite of graphene with nanomaterials potentially acquires much enhanced surface area, thereby increasing the adsorption efficiency. Apart from adsorption, capacitive deionization has also been extensively explored for the desalination of water. This desalination approach offers some unique features which gives it an edge over other existing techniques such as high energy efficiency, environmentally benign nature and no secondary waste generation during the process.[231] Capacitive deionization involves electrostatic adsorption of ions on to the electrode surface. On the application of electric potential difference over electrodes, ions present in the water forms double layer with opposite charge on to the surface of electrode, this ionic layer can be easily desorbed from the electrode by applying an external field after removal of ions from the water, hence no secondary waste generates.[232] Higher surface area and conductivity are the two important properties which govern the capacitive deionization performance of the material[233] and significantly graphene exhibits both of these,

which makes it a suitable electrode material for use in capacitive deionization process.[231–235] Wang *et al.*[234] used graphene as an electrode material for the capacitive deionization of aqueous NaCl solution and monitored change in the conductivity at different time intervals during capacitive deionization. A marked reduction in conductivity of the solution from 86.9 to 10.2 μS cm^{-1} after 120 min was observed. Electrosorptive capacity was found to be 0.88 mg g^{-1}.

3.1. Fe₃O₄/Graphene composite as a adsorbent

3.1.1. Fe₃O₄/Graphene composite as adsorbent for water purification.
The hybrids of graphene with magnetic nanomaterials such as Fe_3O_4 have been extensively exploited for removal of pollutants from water.[236–239] Fe_3O_4 is one of the most frequently used materials for water purification due to its high biocompatibility which ensures safety and also the magnetic properties which makes it easy to collect post treatment. After the adsorption, the Fe_3O_4–graphene composite can be easily separated out from the solution *via* the use of a magnet. However, in continuous flow systems, the poor stability and the ease of further oxidation to Fe_2O_3 α-Fe_2O_3 and γ-Fe_2O_3 are proving to be the major hurdles for its application.[240] These difficulties can potentially be overcome by incorporating the Fe_3O_4 nanoparticles in a graphene matrix. The formation of composite not only enhances the lifetime of Fe_3O_4 nanoparticles but also allows an easy retrieval after the completion of adsorption. After the adsorption, the Fe_3O_4–graphene composite can be easily separated out from the solution *via* the use of a magnet (Fig. 8). Also, the durability of the composite as an adsorbent is dictated by the extent of binding of Fe_3O_4 with graphene surface, which ensures prolonged life time of the adsorbent by retarding the leaching of Fe_3O_4 from composite during water treatment process.

Chandra *et al.*[240] used a magnetite reduced graphene oxide (M-RGO) composite for the removal of Arsenic ions and also studied the effect of pH on the adsorption efficiency of the hybrid material. It was observed that the adsorption efficiency is highly dependent on the pH values. The adsorption mechanism involved electrostatic attraction between positively charged

Fig. 8 Photograph of the fuchsine solution (20 mg L^{-1}, right) and the solution after adsorption with the G/Fe₃O₄ adsorbent for 1 h and separation with a magnet (left). Reproduced with permission from ref. 239.

M-RGO and negatively charged arsenic/arsenous acid (H_3AsO_4). When the pH of the solution was less than the point of zero charge (pH_{pzc}), M-RGO got charged positively thereby, attracting more As(v) anions and leading to an accelerated adsorption of As(v) anions. As the pH of the solution was increased beyond the pH_{pzc} positive charge on M-RGO got reduced but the anionic charge kept increasing due to As(III) anions leading to an increase in adsorption. This is suggestive of the fact that, unlike the adsorption of As(v), the adsorption of As(III) ions on M-RGO is due to surface complexation instead of electrostatic interactions. Liu and co-workers[241] too studied the effect of pH on adsorption of Co(II) on magnetite graphene hybrid. A steady increase in adsorption is observed with an increase of pH from 3 to 6, but the rate of adsorption increased abruptly within the pH range of 6–8.5 and retains high sorption concentration on increasing pH > 8.5. The effects of variation in ionic strength, foreign cations, foreign anions and sorbent content on the sorption of Co(II) ions on magnetite/graphene composite is demonstrated in Fig. 9(a)–(d). Changes in ionic strength influences the outer-sphere complex formation, but in case of Co(II) sorption, the variation in ionic strength exhibited negligible effect on sorption ability of composite towards Co(II) ions (Fig. 9a). This is suggestive of the fact that sorption of Co(II) ion on M-RGO, can be attributed to the inner-sphere surface complexation rather than ion exchange or outer-sphere surface complexation. The presence of foreign cations (K^+, Na^+, and Mg^{2+}) and anions (Cl^-, NO_3^- and ClO_4^-) exhibited notable effect on sorption ability of magnetite/graphene composite (Fig. 9b and c). The order of sorption of Co(II) on composite was found to

be $K^+ > Na^+ > Mg^{2+}$ and $ClO_4^- > NO_3^- > Cl^-$ for cations and anions respectively. On increasing solid content an obvious increment in sorption of Co(II) was observed (Fig. 9d) which was attributed to an increase in sorption sites on increasing solid content. A study by Zhu et al.[242] showed that the removal of the chromium ions by magnetic graphene composite is highly dependent on pH and the composite shows a complete removal of Cr(IV) in acidic pH (1–3). At acidic pH the concentration of $HCrO_4^-$ ions which have higher tendency for adsorption on the composite was dominant over CrO_4^{2-}. The decreased uptake of Cr(VI) species by the composite on raising pH from acidic to basic was attributed to the increased concentration of OH^- ions on the surface of composite, competing with the chromium ions for the available adsorption sites on the composite surface. Similarly, highly acidic solution can also impede the sorption ability of the composite because at high acidic pH, the concentration of hydrogen ions which can compete with the metal ions for the active sites available, exceeds, and can limit the uptake of metal ions by composite.[243,244] Fig. 10(a)–(c) shows UV-Vis spectrum of Cr(VI) solution treated with different loadings of graphene, loadings of magnetite graphene composite and the plot between removal percentage and adsorbent concentration for graphene and magnetite graphene composite. The Fig. 10(a) and (b) clearly show that with an increase in the loading of graphene in the composites, a reduction in the peak intensity is observed, indicative of the removal of Cr(VI) ions. While, graphene only achieves ~44.6% removal efficiency of Cr(IV) even at highest testing concentration (3 g L^{-1}), the magnetite graphene exhibits 100% removal efficiency within 5 min (Fig. 10c).
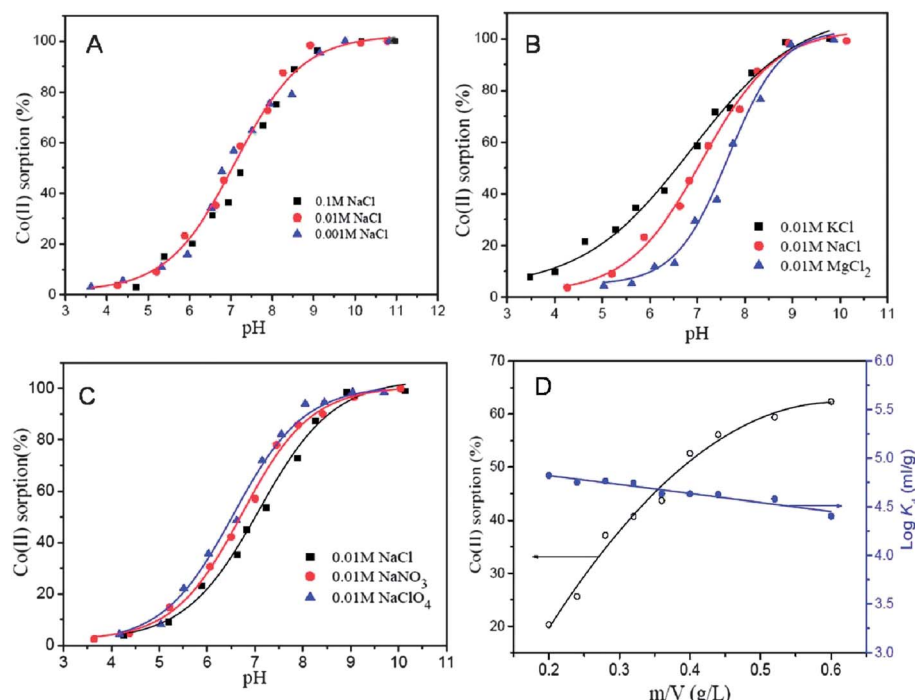

Fig. 9 Effect of ionic strength (A), foreign cations (B), foreign anions (C), and sorbent content (D) on Co(II) sorption onto the M/GO composite, at pH = 6.8 ± 0.1, T = 303.15 K, I = 0.01 M NaCl, $C_{Co(II)\ initial}$ = 10.0 mg L^{-1}. Reproduced with permission from ref. 241, Copyright (2011) American Chemical Society.
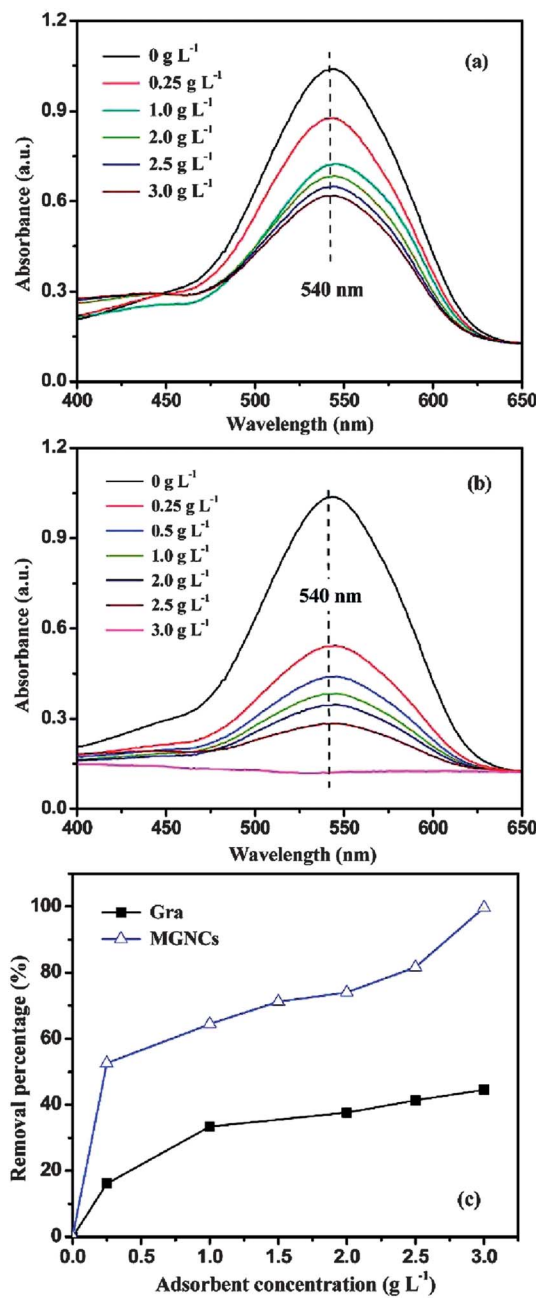
Fig. 10 UV-Vis absorption of the solutions after treated with (a) different loadings of graphene (Gra), (b) different loadings of MGNCs, and (c) Cr(VI) removal percentage based on different loadings of Gra and MGNCs. ([Cr(VI)] = 1000 µg L^{-1}, pH 7, treatment time: 5 min). Reproduced with permission from ref. 242, copyright (2011) American Chemical Society.

Besides the adsorption of heavy metal ions, adsorption of organic pollutants[239,245] on metal oxide/graphene composite has also been investigated. He et al.[246] prepared Fe$_3$O$_4$ graphene composite having covalent binding between Fe$_3$O$_4$ and graphene. The surface of Fe$_3$O$_4$ was modified with tetraethyl orthosilicate and (3-aminopropyl) triethoxysilane (APTES), to attach active amino groups on to the surface of Fe$_3$O$_4$. Furthermore, these active amino groups entangled on the

surface of Fe$_3$O$_4$ were exposed to carboxylic group present on the surface of graphene oxide resulting in the formation of covalent bonds. The as prepared Fe$_3$O$_4$/graphene composite exhibited excellent adsorption capacities of nearly 190.14 and 140.79 mg g^{-1} for methylene blue and neutral red, respectively. Wang et al.[239] reported on the speedy adsorption of organic dye, fuchsine, on the magnetic nanocomposites, wherein, nearly 96% of the dye got adsorbed within 10 minutes. This quick adsorption of fuchsine was attributed to two different types of interaction between graphene and dye molecules, including: (i) Van der Waals interactions between the aromatic backbone of the dye molecule and the hexagonally packed carbon atoms, and (ii) π–π stacking interaction among aromatic part of the dye and the delocalized π-electron system of graphene. Similarly, magnetite/reduced graphene oxide nanocomposites synthesized using solvo-thermal method by Sun et al.[247] demonstrated excellent removal efficiency for Rhodamine B (91%) and malachite green (94%) dyes. For these systems, the crucial parameters affecting the performance of the composites were the loading of Fe$_3$O$_4$ in the composite and the pH of the solution. An increase in the loading of Fe$_3$O$_4$ in composite beyond a certain amount caused a drop in the performance, due to a reduction in the exposed surface area of composite. To evaluate the possibility of real life application for this magnetite/reduced graphene oxide nanocomposite, the authors tested it for purification of industrial waste water having both dyes in combination with other pollutants and noticed that the composite exhibits nearly the same removal efficiency for dyes present in both deionised water and industrial waste water. Li et al. formulated a magnetic CoFe$_2$O$_4$-functionalized graphene composite with adsorption capacity of 71.54 mg g^{-1} towards synthetic dye methyl orange.[248]

3.1.2. Fe$_3$O$_4$/Graphene composite in detection of pollutants in water. Excellent sorption ability of graphene/metal oxide adsorbents has not only been explored for purification of water, but more recently it has also been used for the extraction of trace level pollutants from water for sample preparation for different analytical techniques. Composites of graphene with magnetic nanoparticles are most popular material of choice for this application. There are several studies reporting use of magnetic graphene as extraction media for enrichment of trace level pollutants in samples.[238,249–252] Luo et al.[250] used magnetic Fe$_3$O$_4$/graphene composite for the extraction of six sulfonamides from the water and also optimized various parameters such as pH, graphene content and extraction time. Optimal extraction conditions to achieve maximum efficiency were found to be pH 3, graphene 0.3 mg and an extraction time of 4 min. Wu and co-workers[238] employed graphene based magnetic nanocomposite for the pre-concentration of few carbamate pesticides in environmental water sample. The magnetic graphene composite exhibited good adsorptive ability, strong magnetism and could be reused up to twelve times without any significant loss in sorption capacity. In another study by Zhao et al.,[249] magnetic graphene as an adsorbent in the solid phase extraction procedure for the enrichment of some triazine herbicides in water samples was employed.

3.2. Composite of metal oxides other than Fe_3O_4 with graphene as adsorbent

Apart from Fe_3O_4 various other metal oxides such as SiO_2,[68] ZnO,[253] MnO_2,[254,255] $CoFe_2O_4$ (ref. 248) and ZrO_2 (ref. 256) have also been hybridized with graphene to formulate adsorbents. For large scale application of composites as adsorbents; the selectivity of the adsorbent towards targeted adsorbate is highly desirable. There have been a few reports on the higher selectivity of graphene nanocomposites for certain metal ions.[68,257] The SiO_2/graphene composites prepared by Hao et al.,[68] exhibited excellent selectivity for Pb(II) ions out of several available divalent ions such as Cu^{2+}, Ni^{2+}, Co^{2+}, Cd^{2+} and Cr^{3+}. However, an enhancement in the ionic strength of the solution by adding salts such as KNO_3 suppressed the adsorption efficiency of the composite, as these salts compete with the metal ions for the available adsorption sites on the surface of composites. Lee and Yang[258] studied the effect of hydrothermal treatment period on the adsorption efficiency of the TiO_2 blossoms/graphene composite for the removal of Zn^{2+}, Cd^{2+} and Pb^{2+} ions. On extending the length of hydrothermal treatment period from 6 h to 12 h, the surface area of the composites was enhanced from 88.97 to 132.74 $m^2\,g^{-1}$ and adsorption efficiency from 44.8 ± 3.4 to 88.9 ± 3.3 $mg\,g^{-1}$ for Zn^{2+}, 65.1 ± 4.4 to 72.8 ± 1.6 $mg\,g^{-1}$ for Cd^{2+}, and 45.0 ± 3.8 to 65.6 ± 2.7 $mg\,g^{-1}$ for Pb^{2+}, respectively. Zong and co-workers[256] obtained ZrO_2 functionalized graphite oxide by post-grafting method and employed it as a sorbent material for the removal of phosphate ions. Again, the adsorption capacity of phosphate ions on ZrO_2 functionalized graphite oxide was found to be highly dependent on the pH values and diminished on increasing the pH value from 2–12 and attained its maximum at a pH value of 2.03. This reduction in the adsorption capacity on increasing pH was explained on the basis of variation in the extent of various types of interaction between phosphate ions and ZrO_2/graphene composite including electrostatic interaction, ion-exchange and acid base interaction. Nanocomposite of hydrated zirconium oxide with graphene oxide prepared by Luo et al. show excellent adsorption capacities 95.15 and 84.89 $mg\,g^{-1}$ for As(III) and As(v) ions, respectively. These values were nearly 3.54 and 4.64 times higher than pristine $ZrO(OH)_2$ nanoparticles.[259] Li et al.[260] reported defluoridation of aqueous solution using manganese oxide coated graphene oxide and also studied the effect of different parameters such as pH, adsorbent dose, contact time and temperature on adsorption behaviour of composite. Manganese oxide/graphene oxide composite exhibited maximum adsorption efficiency at pH 5.5. On increasing the adsorbent dosage from 5 to 65 mg per 50 mL, the adsorption percentage was also enhanced from 6 to 45%. An increase in adsorbent dosage enhanced the adsorbent percentage, but reduced the overall adsorption capacity, as the increase in the dosage beyond the threshold amount resulted in unsaturated reactive sites, lower surface area and increased diffusion path length. On the other hand, at lower dosage all active sites got occupied by the adsorbate, thereby enhancing the adsorption capacity. However, it should be noted that the mechanism involved in the adsorption of heavy metal ions on graphene supported metal oxide nanoparticles is not clear and under investigation. Recently, Ren et al.[261] have performed a detailed characterization study of δ-MnO_2/graphene samples before and
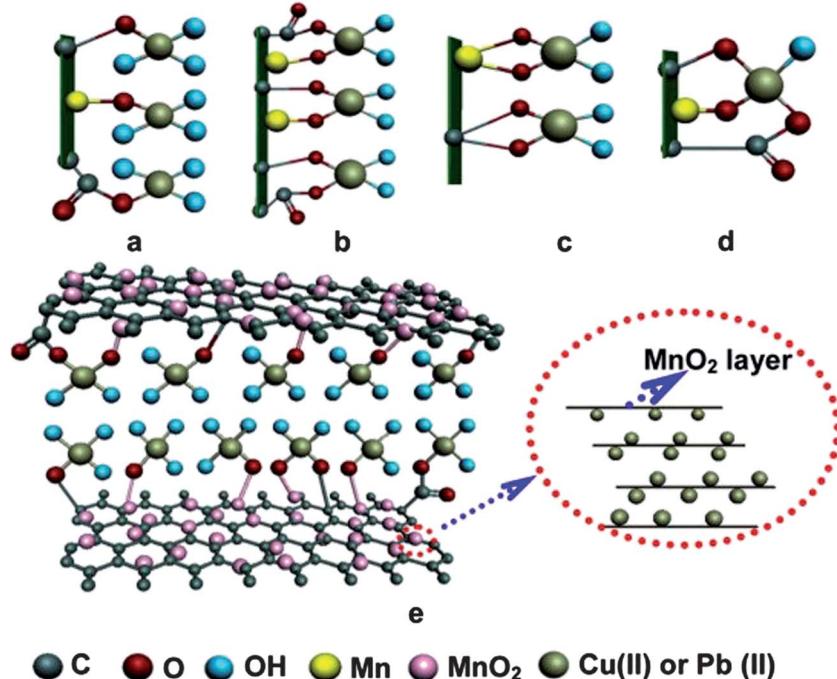

Fig. 11   Possible tetradentate configurations after Cu(II) and Pb(II) sorption: (a) monodentate, (b) bidentate mononuclear, (c) bidentate binuclear, (d) multidentate, and (e) proposed tetradentate monodentate complexes on GNS/MnO_2 surface and MnO_2 layer in actual solution. Reproduced with permission from ref. 261.

after adsorption of copper and lead ions on it and have proposed a possible mechanism for the adsorption. Their results revealed that initially, the protonation of functional group may take place and surface oxygen of different groups C–OH, Mn–OH or –COOH groups which can behave as lewis acid and forms tetradentate monodentate complexes with Cu(II) and Pb(II) ions which are lewis base in nature. Also, the disappearance of some of the characteristic peaks of δ-MnO$_2$ from X-ray diffractogram after the adsorption provides evidence that metal ions not only get adsorbed on to the surface of composite but also intercalate in the interlayer of δ-MnO$_2$ and thereby enhancing the disorder in the structure. Fig. 11 shows suggested mechanism involved in adsorption of Cu(II) and Pb(II) ions on δ-MnO$_2$/graphene. The δ-MnO$_2$/graphene showed excellent cycling as well and it was observed that the material can be used for at least four times, without any significant loss in the sorption ability. In a similar work, Ren *et al.*[262] studied the adsorption of nickel ions on graphene/δ-MnO$_2$ nanocomposite and noticed a significant effect of temperature upon extent of sorption of nickel ions on the nanocomposites. On increasing the reaction temperature from 298 K to 318 K, the adsorption capacity of graphene nanosheets/δ-MnO$_2$ composite was enhanced from 46.55 to 60.01 mg g^{-1}. The adsorption capacity of the graphene/δ-MnO$_2$ composite was observed to be 1.5 and 15 times higher than for δ-MnO$_2$ and graphene nanosheets respectively.

The two most crucial attributes which an adsorbent material should show are durability and reusability; and significantly, graphene based nanocomposites shows both these properties. There are several studies reporting on the regeneration of graphene based composites with minimal loss of performance.[47,54,237,256,263] Fig. 12 shows the variation of the sorption efficiency upon multiple regeneration rounds for the removal of U(IV) by Fe$_3$O$_4$/GO.[237] It can be clearly observed that that even after six regenerations, the regenerated Fe$_3$O$_4$/GO maintained good sorption efficiency. Out of various types of metal oxides/graphene based adsorbent few examples are compiled in Table 3.
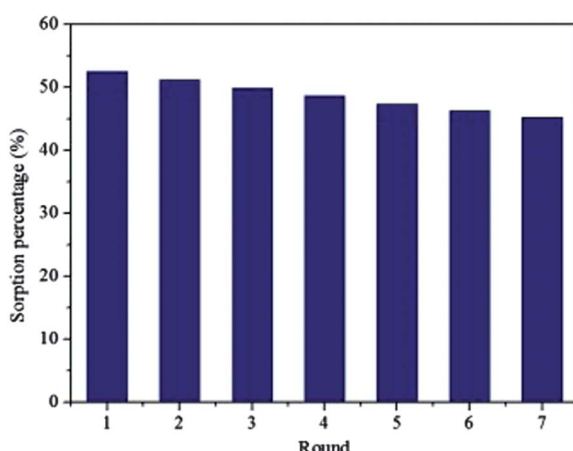
Fig. 12 Recycled efficiency of Fe$_3$O$_4$/GO in the removal of U(VI). $T = 293$ K, pH $= 5.5 \pm 0.1$, $C_{U(VI)initial} = 1.12 \times 10^{-4}$ mol L^{-1}, m V$^{-1} = 0.3$ g L^{-1}, $I = 0.01$ mol L^{-1} KNO$_3$ Reproduced with permission from ref. 237.

3.3. Proposed strategies for improving adsorption efficiency of metal oxide/graphene composites on the basis of aforementioned studies

Owing to low density and high surface area of graphene, its addition to the composite increases the surface area without a significant increase in the weight so adjustment of exact weight ratio between metal oxide graphene is crucial. While in photo-catalytic applications, the semiconductor metal oxide particles control the photocatalytic activity of composite; the sorption capacity is largely dictated by the graphene content. Ample studies have reported on the reduction in the adsorption capacity of the composites upon an increase in the amount of metal oxide beyond a critical limit. Since metal oxides are comparatively heavy and posses lower surface area to weight ratio as compared to graphene, so an inordinate increase in the amount of metal oxide in the composites, results in a reduction of the adsorption capacity.

The adsorption capacity of the materials for heavy metal ions, organic molecules such as dyes and other pollutants is highly dependent on the pH value and hence maintaining a pH which favors adsorption is absolutely crucial. An increase in the pH value can enhance the concentration of hydroxyl groups on the surface which can hinder adsorption of metal ions; on the other hand, highly acidic pH can increase the concentration of H$^+$ ion in the solution which compete with metal ions for the sorption sites available on the adsorbent so maintaining a pH at which both performance retarding side reactions can be prevented is highly desirable. Some heavy metal ions such as chromium and arsenic form different metastable species at different pH levels and out of these various metastable species few may acquire compatibility and can be easily adsorbed on adsorbent which increases the adsorption capacity of the composite.

Along with a high activity, the durability is an important issue which needs to be resolved to provide real life applications for metal oxide/graphene based adsorbents. Loose physical adhesion or weak and labile bonding between metal oxide and graphene can result in the leaching of metal oxide in to the treated water which can not only reduce the life time of the adsorbent but also can cause cross contamination of the water. Thus, the strength of bonding between metal oxide and graphene is a matter of great concern and synthesis route, reaction conditions and nature of reactants, which can facilitate a firm bonding between the metal oxide and graphene must be chosen. Surface of the metal oxide and graphene can be modified with functional groups which can help in attaining tight binding between metal oxide and graphene.

As adsorption is a superficial phenomenon, hence, the surface properties of the adsorbent play very important role in deciding its sorption ability. It has been found that presence of active groups such as –COOH and –OH on to the surface of the graphene contributes significantly to its sorption capacity by forming complexes with metal ions. Therefore, an enhancement in the number of active groups on the surface increases sorption capacity. Furthermore, the surface of graphene can be modified with some other groups such as –NH$_2$, which can readily combine with the metal ions in the solution. Not only the functionalities present on the surface of the support interact with the metal ions, but the

Table 3 Different metal oxide/graphene and graphene oxide composites used as adsorbents for water purification

Graphene composite	Surface area	Adsorption capacity	Targeted pollutant	Ref.
FeO˙ Fe$_2$O$_3$/GO	272.59 m^2 g^{-1}	2.85, 2.70 and 5.72 mmol g^{-1}	1-Naphthylamine, 1-naphthol, and naphthalene	245
ZrO$_2$–GO	160.1 m^2 g^{-1}	16.45 mg g^{-1}	Phosphate ions	256
MgAl-layered double hydroxides/GR	34.97 m^2 g^{-1}	172.55 mg g^{-1}	Cr(IV)	264
Fe$_3$O$_4$/chitosan/GR	392.5 m^2 g^{-1}	95.31 mg g^{-1}	Methyl blue	60
Fe$_3$O$_4$/chitosan/GO	382.5 m^2 g^{-1}	76.94 mg g^{-1}	Pb^{2+}	66
Mn$_3$O$_4$/GO	108 m^2 g^{-1}	11.93 mg g^{-1}	Fluoride	260
Fe$_3$O$_4$/GO	145.8 m^2 g^{-1}	0.708 mg g^{-1}	2,4,40-Trichlorobiphenyl (PCB 28)	265
Fe$_3$O$_4$/GR		202.84–375.94 mg g^{-1} 35.47–43.86 mg g^{-1}	Aniline and p-chloroaniline	63
Fe$_3$O$_4$/GO	—	40 mg g^{-1}	Polycyclic aromatic hydrocarbons	266
TiO$_2$/GO	132.74 m^2 g^{-1}	88.9 ± 3.3 mg g^{-1} 72.8 ± 1.6 mg g^{-1} 65.6 ± 2.7 mg g^{-1}	Zn^{2+}, Cd^{2+} and Pb^{2+}	258
Fe$_3$O$_4$–cyclodextrin–chitosan/GO	445.6 m^2 g^{-1}	53.48 mg g^{-1}	Hydroquinone	61
Fe$_3$O$_4$/GO	—	69.49 mg g^{-1}	U(VI)	237
δ-MnO$_2$/GR	—	46.6 mg g^{-1}	Ni(II)	262
Fe(OH)$_3$/GO	—	23.78 mg g^{-1}	Arsenate	267
GR–Fe$_3$O$_4$	—	—	Carbamate pesticides	238
Fe$_3$O$_4$/GR	—	89.4 mg g^{-1}	Fuchsine	239
Fe$_3$O$_4$/GR	256 m^2 g^{-1}	198.23 mg g^{-1}	Pararosaniline solution	268
Fe$_3$O$_4$/GR	—	43.82 mg g^{-1}	Methylene blue	263
Fe$_3$O$_4$–RGO–MnO$_2$	133.0 m^2 g^{-1}	14.04 mg g^{-1} and 12.22 mg g^{-1}	As(III) and As(v)	269
Magnetic cyclodextrin/chitosan/GO	445.6 m^2 g^{-1}	67.66 mg g^{-1}	Cr(IV)	270
Magnetic GR	42.1 m^2 g^{-1}	1.03 mg g^{-1}	Cr(IV)	242
RGO–ZrO(OH)$_2$	420 m^2 g^{-1}	95.15 and 84.89 mg g^{-1}	As(III) and As(v)	259
CoFe$_2$O$_4$/GR	330 m^2 g^{-1}	101.34 mg g^{-1}	Methyl orange	248
Metal/metal oxide (MnO$_2$)/GO	—	—	Hg(II)	271
Titanate/GO	>350 m^2 g^{-1}	~83.26 mg g^{-1}	Methylene blue	272
SiO$_2$/GR	252.5 m^2 g	113.6 mg g^{-1}	Pb(II)	68
MFe$_2$O$_4$, M = Mn, Zn, Co and Ni/RGO	—	23 and 35 mg g^{-1}	Rhodamine B and methylene blue	273
δ-MnO$_2$/GR	—	1620 and 781 μmol g^{-1}	Cu(II) or Pb(II)	255
GO/MnO$_2$	—	—	Ammonia	254
(Mn$_x^{2+}$Fe$_{2-x}^{3+}$O$_4^{2-}$) (IMBO)–GR	280 m^2 g^{-1}	14.42 mg g^{-1}	As(III)	274
Fe$_3$O$_4$/RGO	148 m^2 g^{-1}	~5 and 13 mg g^{-1}	As(III) and As(v)	240
ZnO/GO	—	32.6 mg g^{-1}	Rhodamine B	253
Magnetite/RGO	—	12.98 mg g^{-1}	Co^{2+}	241
GO/Fe$_3$O$_4$	—	18.26 mg g^{-1} and 19.09 mg g^{-1}	Cu^{2+} and fulvic acid	275
Fe$_3$O$_4$/GO	—	91.29 mg g^{-1}, 64.23 mg g^{-1} and 20.85 mg g^{-1}	Cd(II), methylene blue and orange G	276
Magnetic/GO	—	39.1 mg g^{-1}	Tetracyclines	277
Sulfonated Fe$_3$O$_4$/GO	92.79 m^2 g^{-1}	62.73 mg g^{-1}	Cu(II)	278
Fe$_3$O$_4$/RGO	—	18.22 and 22.20 mg g^{-1}	Ciprofloxacin and Norfloxacin	279
Fe$_3$O$_4$/SiO$_2$/GO	—	111.1 mg g^{-1}	Methylene blue	280
Fe$_3$O$_4$/RGO	—	13.15 and 22 mg g^{-1}	Rhodamine B and malachite green	247
Fe$_3$O$_4$/GR	~165 m^2 g^{-1}	4.86, 3.26, and 6.00 mg g^{-1}	Cr(VI), As(v), and Pb(II)	281
Mg–Al layered double hydroxide/GO	35.4 m^2 g^{-1}	183.11 mg g^{-1}	As(v)	282
Fe$_3$O$_4$/GO	—	425 mg g^{-1}	Reactive black 5	283
Fe$_3$O$_4$/GR sheets	93.7 m^2 g^{-1}	73.26 mg g^{-1}	Methylene blue	284
Fe$_3$O$_4$/GO	—	167.2 and 171.3 mg g^{-1}	Methylene blue (MB) and neutral red (NR)	285
Fe$_3$O$_4$/GO	43.56 m^2 g^{-1}	32.33 mg g^{-1}	Cr(VI)	286
Fe$_3$O$_4$/RGO	164.96 m^2 g^{-1}	40.01 mg g^{-1}	Rhodamine B	287
Fe$_3$O$_4$/RGO	272.59 m^2 g^{-1}	454.55 mg g^{-1} and 303.03 mg g^{-1}	Pb(II) and Naphthylamine	288
Fe$_3$O$_4$/GO	—	188 mg g^{-1}	Reactive black 5	289

functional groups on the semiconductor nanoparticles also interact with the metal ions of pollutant. Hence, synergistic effects can be expected in the case of dual functionalized catalyst and support, for example functionalized semiconductor nanoparticles on reduced graphene oxide (which retains some –OH and –COOH and –C–O–C– groups even after reduction).

The removal of the adsorbent, post water treatment, from the purified water remains a considerable issue with traditional adsorbents. The introduction of magnetic adsorbent materials in composites makes them easier to be separated from the purified water; thus providing an edge to the magnetic metal oxide containing composite on nonmagnetic metal oxides. After completion of adsorption, magnetic adsorbent can easily be recovered from the treated water using an external magnet, which eliminates the risk of cross contamination.

A good adsorbent should not only be quick in adsorption of pollutants but should also exhibit speedy and complete desorption of pollutants during regeneration, for it to be reused. Ease of regeneration of adsorbent decides its wide scale applicability. The desorption of pollutants can be carried out by adjusting the pH of the solution to a value which impedes adsorption. Replacement of metal ions by H^+ ions through acid treatment can be another way to regenerate the absorbent. For organic pollutants, such as dyes and pesticides, regeneration can be carried out by simply washing composite with a solvent to dissolve away the pollutants. Heat treatment can also be an attractive option for regeneration of the adsorbent if adsorbent is stable at higher temperatures.

4. Graphene/metal oxide composites for antimicrobial treatment

Pristine graphene oxide and graphene without any functional additives have also been explored as antimicrobial agents.[73,290–295] It was observed that the lateral dimensions and morphology of the graphene oxide sheets play a key role in its efficacy as antimicrobial agent; with the larger sheets exhibiting higher antimicrobial activity due to extensive coverage of the cell surfaces by them, as compared to the smaller sheets. This complete warping of bacterial cells by larger graphene sheets (>0.4 μm^2) blocks all the available active sites, thereby disallowing the cell proliferation. On the other hand, smaller sized graphene oxide sheets (<0.2 μm^2) do stick to the cell membrane; but they are not capable of occupying and isolating the whole cell surface, there by their efficiency is reduced significantly.[72] Fig. 13 shows the AFM images of *Escherichia coli* (*E. coli*) cells incubated with larger and smaller graphene oxide sheets. Fig. 13(a) and (b) shows the *E. coli* cells incubated with deionized water for 2 h which is not showing any effect on *E. coli* cells. Fig. 13(c, d) and (e, f) shows the coverage of *E. coli* cells with larger graphene oxide sheets (GO-0) and smaller graphene oxide sheets (GO-240) respectively. The surface roughness value exhibited by *E. coli* cells is shown in Fig. 13(a, c and e) were found to be 4.78 ± 0.82, 2.18 ± 0.46, and 14.80 ± 3.19 nm, respectively. Fig. 14(a) illustrates wrapping of bacteria by graphene sheets. The aggregation of graphene oxide sheets can also impede its antimicrobial activity; as well dispersed graphene oxide sheets can show better antimicrobial activity because of higher exposed surface area.[70] Ahmed and co-workers[292] have investigated the effect of graphene oxide on wastewater borne microbial community. Results have corroborated the fact that the graphene oxide impairs the metabolic activity of the microorganism, thereby restricting the cell proliferation and ultimately causing the cell death. Reduced metabolic activity causes a reduction in the consumption of oxygen which reduced the value of biological oxygen demand (BODs). Reactive oxygen species generated by graphene oxide was also responsible for microbial cell inhibition. Graphene oxide has also been shown to hinder the activity of ammonia
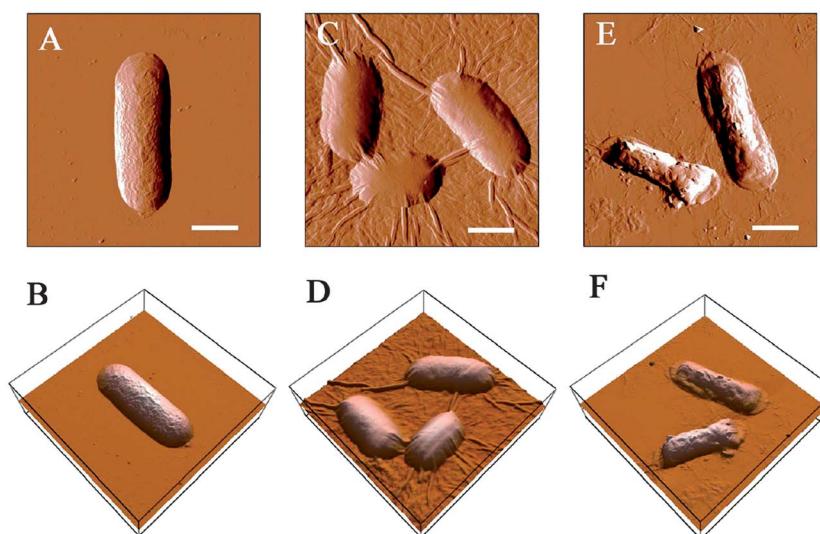

Fig. 13 AFM amplitude and 3D images of *E. coli* cells after incubation with GO sheets. (A and B) *E. coli* incubation with deionized water for 2 h, (C and D) *E. coli* incubation with the 40 μg mL^{-1} GO-0 suspension for 2 h, and (E and F) *E. coli* after incubation with the 40 μg mL^{-1} GO-240 suspension for 2 h. The scale bars are 1 μm. Reproduced with permission from ref. 72, Copyright (2012) American Chemical Society.
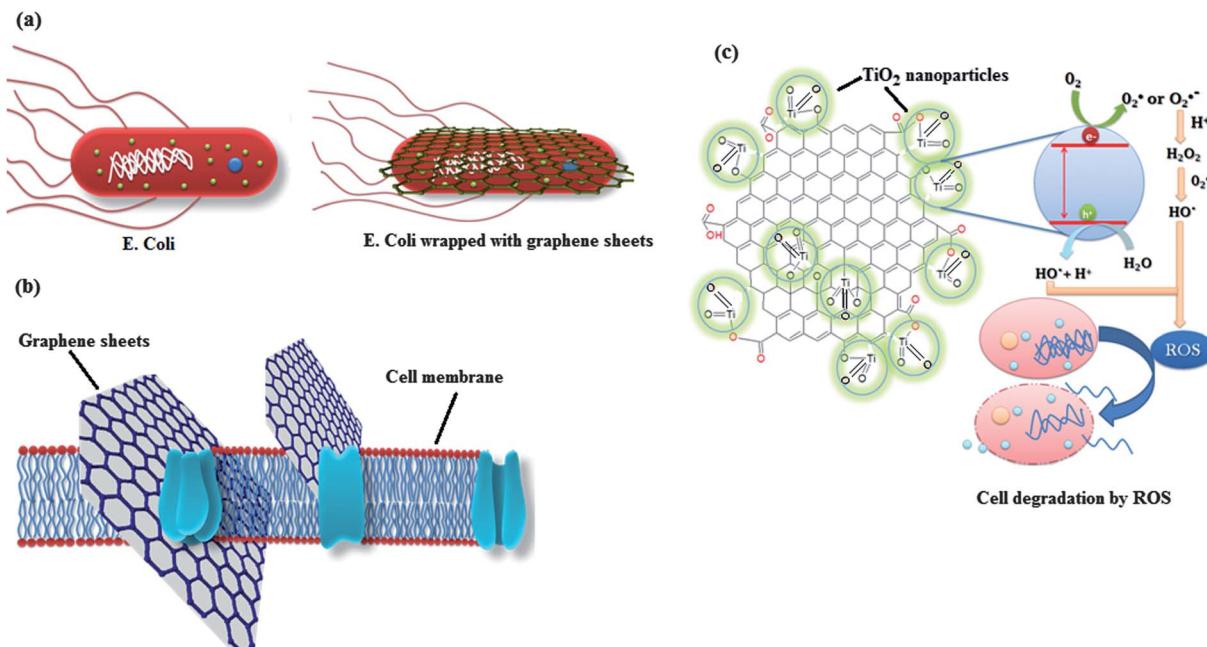
Fig. 14 (a) Wrapping of *E. coli* by graphene sheets. (b) Slicing of cell membrane by sharp edges of graphene. (c) Mechanism involved in photo-inactivation of cells by metal oxide/graphene composite.

oxidizing bacteria and polyphosphate accumulating organisms, which are the responsible for the removal of the following two nutrients; nitrogen (as NH_3–N) and phosphorous (as PO_4^-) from waste water. However the antibacterial activity of graphene derivatives is not entirely accepted there are few reports in the literature which contradict with the proposed antibacterial property of graphene. Ruiz *et al.*[296] investigated the antibacterial activity of the graphene oxide and observed an increase in the bacterial cell proliferation instead of reduction in cell growth which suggests that graphene oxide is neither bactericidal nor bacteriostatic material. It was concluded that graphene oxide (GO) sheets serves as scaffold for the cell surface attachment and proliferation. Graphene oxide (GO) films also did not exhibit any cytotoxic effects on the mammalian cells, which gives an edge to graphene over carbon nanotubes which have been found to be toxic at different concentrations.[297,298] The authors have suggested that the introduction of contaminants in to the graphene oxide films during preparation might be a reason behind the observed antimicrobial activity of the graphene reported in various studies. Therefore a preparation method which can yield pure and quality graphene material is highly desired to completely and fully understand antimicrobial activity of graphene. Apart from selection of preparation method for graphene, investigations to find out minimum inhibitory concentration (MIC) and suitable dosage amount of graphene for antimicrobial applications is also very much important. Krishnamoorthy *et al.*[290] investigated antibacterial activity of graphene sheets against four different pathogenic bacteria *Escherichia coli*, *Salmonella typhimurium*, *Enterococcus faecalis* and *Bacillus subtilis* and also optimized the minimum inhibitory concentration (MIC) values. The MIC value was found to be 1 μg mL^{-1} against *Escherichia coli* and *Salmonella typhimurium* and 8 μg mL^{-1} and 4 μg mL^{-1} for *Enterococcus faecalis*

and *Bacillus subtilis* respectively. Antibacterial activity of graphene sheets was compared with antibiotic kanamysin and found to be superior. In most of the studies to understand effects of graphene on living beings microorganisms such as bacteria and viruses have been chosen as model species however, the effect of exposure of graphene on large animals is yet to be ascertained. As compared to the photocatalytic and adsorptive applications, the antimicrobial applications of graphene/metal oxide composites have been comparatively less explored and hence, there is the need and huge potential to undertake a lot of detailed studies to explore and understand their anti-microbial behaviour. Some of the recently published literature is discussed in the following sections.

The composites of graphene and reduced graphene oxide hybrids with metals and metal oxides such as Ag, Fe, Fe_3O_4 and TiO_2 have been explored as an antimicrobial agent for the disinfection and sensitization of water. Recently Gollavelli and co-workers[281] have synthesized Fe_3O_4 graphene composite and demonstrated the good disinfection properties against *E. coli*, while maintaining low toxicity towards zebrafish. The antibacterial activity of magnetic graphene was attributed to the high surface roughness and consequential piercing of cell membrane by graphene and the bactericidal action of Fe_3O_4 nanoparticles. Fig 14(b) shows slicing of cell membrane by the sharp edges of graphene which destroys the cell integrity by draining out the cell contents resulting in cell death. Akhavan *et al.*[299] reported that graphene oxide/TiO_2 thin films annealed at 400 °C can photo-inactivate *E. coli* 25% more efficiently, as compared to bare TiO_2. In this case, graphene oxide served as an electron acceptor for the removal of electron from electron hole pair generated upon exposure of photoactive material to light. Simultaneously, the quantum efficiency of the photocatalysis was enhanced *via* an increase in the life time of the hole and a

reduction in the electron–hole recombination. The graphene oxide/TiO$_2$ thin films exhibited significantly improved antibacterial activity by factors of 7.5, 3.7, 1.7 and 1.1, as compared to unsupported TiO$_2$, Ag–SiO$_2$, Ag nanorods and Ag–TiO$_2$/Ag/a-TiO$_2$ films respectively. Other than nanocrystals, one dimensional nanomaterials such as nanorods, have also been utilized in combination with graphene oxide for photocatalytic degradation of micro-organisms. Liu et al.[300] prepared TiO$_2$ nanorod hybrids with graphene oxide and investigated their bactericidal activity by monitoring the effect of solar radiation exposure on the E. coli bacterial colony, in the presence of hybrid material. The TiO$_2$ nanorod/graphene oxide composite showed significantly higher bacteriocidal activity as compared to the TiO$_2$ nanoparticles/graphene oxide hybrid. TiO$_2$ nanorod/graphene oxide composite inactivated 90% E. coli within 27 min but TiO$_2$ nanoparticles/graphene oxide hybrid took 52 min to achieve same performance. Cao et al.[301] have reported that TiO$_2$/graphene composite with 4.2 wt% graphene shows photoactivity in visible spectrum as well, which was attributed to formation of Ti–C bond between TiO$_2$ and graphene. The photocatalytic activity of TiO$_2$/graphene composite was tested against E. coli and it was observed that in the absence of visible light, the TiO$_2$/graphene composites were inactive. However, on illumination with visible light, the composite showed excellent antibacterial activity and upon a 12 hours exposure of visible light, the bacterial cell viability was reduced up to 9.5%. Kavitha and co-workers[212] tested the bactericidal activity of ZnO/graphene composite against E. coli. The incubation of ZnO/graphene composite with E. coli cells for 12 hours declined 100% of E. coli cells in the medium.

Besides metal oxides, other semiconductor nanoparticles in combination with graphene such as CdS,[302] Ag$_3$PO$_4$[303] and Bi$_2$MoO$_6$[304] etc. have also been explored as antimicrobial agents. Gao et al.[302] have studied the antibacterial activity of CdS/graphene oxide nanocomposites for inhibiting the growth of both gram positive (Bacillus subtilis) and gram negative bacteria (E. coli). The CdS/graphene oxide nanocomposites killed nearly 100% of the E. coli bacteria within 25 min of visible light exposure. On the other hand, bare unsupported CdS nanoparticles without any graphene oxide, only killed 55% of the bacteria in the same duration. The CdS/GO composites showed slightly higher antibacterial efficiency against gram positive bacteria (Bacillus subtilis) as compared to gram negative bacteria, E. coli. This was ascribed to the presence of complex membrane structure, comprising of an additional outer membrane which protects the inner layer from the attack by active radical species, as opposed to a much more simple membrane structure in gram positive bacteria. Akhavan et al.[305] employed WO$_3$/graphene composites for the protein degradation and ribonucleic acid (RNA) efflux of viruses. It was found that WO$_3$ itself did not exhibit any significant effect on viruses even in the presence of visible light, but the composite of WO$_3$ with graphene resulted in a marked improvement of the photodegradation efficiency of WO$_3$ of viral proteins. The photocatalytic activity displayed by WO$_3$/graphene composite was attributed to the formation of W–O–C and W–C bonds, between WO$_3$ and graphene, which facilitated the flow of electron from the WO$_3$ to graphene; thereby extending the life time of charge carriers and limiting the electron hole recombination. The cytotoxicity of graphene/TiO$_2$ composite in miniscule animal C. elegans nematodes was investigated by Akhavan and co-workers.[306] Nearly 98.4% of the nematodes were inactivated within 4 hours of solar radiation exposure with TiO$_2$/graphene composite having ratio of surface area to volume (S/V) of 10. It was further revealed that the major inactivation of the nematodes was due to the interaction between reactive oxygen species (ROS) generated by the composite, instead of the depletion of E. coli count which served as the feed for the nematodes. The percentage of surviving bacteria in the culture media showed an inverse relationship with the surface area to volume (S/V) ratio.

Table 4 Different metal oxide/graphene and graphene oxide composites used as antimicrobial agents

Graphene composite	Particle size	Graphene content	Antibacterial performance	Targeted Microorganism	Ref.
TiO$_2$/GR sheets	6–12 nm	4.2%	% of surviving bacteria = 9.5%	E. coli	301
TiO$_2$/GO nanosheets	—	—	Antibacterial activity = 65×10^{-3} min^{-1}	E. coli	299
TiO$_2$/GR	10 nm	—	Inactivation of 98.4% nematodes	Caenorhabditis elegans nematodes	306
TiO$_2$/GO nanorods	3–5 nm diameter 25–50 nm length	40%	90% inactivation within 27 min	E. coli	300
ZnO/GR	22 ± 6 nm	0.1%	After 12 h incubation with ZnO/GR resulted 100% reduction	E. coli	212
Ag$_3$PO$_4$/GO	500 nm	17%	100% loss of bacterial viability after incubation of E. coli with 20 mg l^{-1} Ag$_3$PO$_4$/GO	E. coli	303
WO$_3$/GR	15 nm	—	Inactivation of more than 99.999% ($\sim$5 PFU mL^{-1}) viruses under visible light irradiation for 3 h	Bacteriophage MS2 viruses	305
CdS/GR	5–6 nm	—	Inactivation of 100% E. coli within 25 min and 90% of B. Subtilis in 10 min	Bacillus subtilis, Escherichia coli	302
Ag–ZnO/RGO	—	—	Cell concentration reduced from 10^7 CFU mL^{-1} to < 10 CFU mL^{-1} after 80 min UV irradiation	E. coli	186

Fig. 13(c) demonstrates the mechanism involved in photo-inactivation of bacteria by graphene/metal oxide composite.

Besides metal oxide nanoparticles, Ag nanoparticles in combination with graphene or graphene oxide have also been extensively explored as antimicrobial agents.[307–311] As Ag itself exhibits excellent antibacterial activity and is a well established antibacterial agent; the composites of Ag with graphene derivatives should provide enhanced antimicrobial activity. While metal oxides such as ZnO, TiO_2 and Fe_3O_4 have been used as antimicrobial agents the search for metal oxide, which can outperform Ag, is still on. With Ag based disinfectants; high cost is one of the major issues which probably can be overcome by the low cost and ease of availability of metal oxides (Table 4).

4.1. Proposed strategies for improving disinfection property of metal oxide/graphene composite on the basis of aforementioned studies

The antimicrobial activity of pristine graphene and graphene oxide has been shown to be directly dependent on the size of the graphene sheet. Graphene films with of larger size exhibits higher antimicrobial activity as compared to the smaller graphene sheets, and hence, the use of larger graphene sheets for antimicrobial materials, is recommended so that graphene can envelope the cell completely. Thus, for antibacterial applications, the fabrication methods should be chosen as such, which are capable of producing large graphene sheets such as chemical vapor deposition,[312,313] thermocatalytic decomposition,[314] burn–quench method[315] arc discharge method[316] and solid exfoliation[317] etc. Also, graphene sheets possess tendency to wrap up and form agglomerates which reduces their size and consequently their efficiency. Thus, the modification of surface of graphene with molecules and functional groups, which can effectively prevent the folding of the sheets and help in maintaining a stable dispersion are crucial. Also, the presence of certain active groups such as –COOH and –OH, increases the surface roughness; thereby enhancing the antimicrobial activity by damaging the outer membrane of cells through attrition and rubbing. Increasing number of active groups on the surface of the graphene can be an effective way to improvise antimicrobial activity of the graphene based composite. Sharp extremities of the graphene sheets also contribute to its antimicrobial activity; wherein the atomically sharp edges can slice through the cell membrane. Therefore, specific structures and morphologies, which provide a high degree of edge planes, are important.

Reactive oxygen species mediated inactivation of microbial cells using metal oxide/graphene catalyst is also a frequently tried approach. Strategies such as closer interfacial contact between metal oxide and graphene, use of graphene with lower defects, uniform distribution of metal oxide nanoparticles on graphene sheets and use of optimized graphene content in composite, which enhance the photocatalytic activity of the metal oxide/graphene composite can also be adopted for preparation of metal oxide/graphene composite based antimicrobial agents having photocatalysis as working phenomenon.

5. Conclusions and outlook

In summary, various types of metal, metal oxide/graphene composites have been explored for the design of novel and futuristic materials for photocatalysis, adsorption and

Metal oxide with graphene as photocatalyst	Metal oxide with graphene as adsorbent	Metal oxide with graphene as disinfectants
Functions of graphene • Graphene reduces electron hole recombination by acting as electron acceptor. • Graphene facilitates the interaction between metal oxide and organic pollutants by π-π stacking. • Graphene expands the absorption range of metal oxide from UV to visible region. • Graphene keeps metal oxide nanoparticles dispersed hence retards agglomeration.	**Functions of graphene** • Graphene enhances the surface area of the composite. • Graphene acts as support material for metal oxide and avoids leaching of metal oxide during the water treatment process. • Graphene increases mechanical strength of adsorbent. • Graphene facilitate the adsorption of organic molecule having aromatic moities in their structure by π-π interaction.	**Functions of graphene** • Sharp edges of graphene sheets damages the cell membrane of micro-organism. • Covers the micooraganism and isolate it from the external environment. • In photocatalysis asisted antimicrobial process serves as electron acceptor. • Impairs with metabolic pathway of cells.

Benefits of graphene/metal oxide composite:
Longevity, innocuous nature , robustness, easy recycling, enhanced adsorptivity, extended light absorption range, suppressed charge carrier recombination.

Fig. 15   Roles of graphene in improving photocatalytic activity, adsorptivity and antimicrobial activity of the composite and its possible benefit.

disinfectant properties. The coupling of graphene with photo-active metal oxide semiconductors *synergistically* enhances the photocatalytic activity of metal oxide for the degradation of various waterborne pollutants such as organic dyes, heavy metal ions and pathogens. The unique properties of graphene, in conjunction with size-dependent properties of nanomaterials induces further functionalities to the composites such as high adsorption capacity, extended light absorption range and improved charge separation properties along with high stability. The features which graphene endows to the composite and role of it in improving photocatalytic activity, adsorptivity and antimicrobial activity of composite are shown in Fig. 15. Some of the crucial requirements for highly active semi-conductor photocatalysts are: (i) a band gap of ~2.0 eV, for visible light catalysis; (ii) water oxidation (H_2O/O_2) and reduction potentials (H^+/H_2) must lie between the minimum of conduction band (CBM) and maximum of valence band (VBM), (iii) high surface area facets and (iv) ability to overcome the recombination of photoinduced charge carriers.[318,319] A wide variety of growth methods now exist for both *in situ* and *ex situ* processing of metal oxide nanoparticles on graphene and graphene derivatives. However, some existing challenges need to be overcome before large scale implementation of these composites can happen. The technology for synthesis of high quality graphene is not fully mature, and the precise control on the final product in terms of purity, control of defects and defect sites, number of layers and re-aggregation is yet to be established. As discussed in the previous sections, for particular applications, say anti-microbial applications; an edge-dominated structure is much more efficient than planar/epitaxial graphene and hence a suitable preparation method, say plasma enhanced chemical vapour deposition process is required to achieve the product. Similarly, for heavy ion removal by adsorption techniques, high surface area architectures such as aerogels, xerogels based on graphene should be implemented. The micro, nanoporosity of the structures along with the high surface area of graphene lends itself for high adsorption capabilities of heavy metal ions, organic dyes and possible hydrocarbon spills. Also, low-dimensional layered carbonaceous materials such as g-C_3N_4, with an optical band gap of ~2.7 eV have been shown to have promising photocatalytic properties. It has been shown previously that by controlling the ratio of the sp^2 to sp^3 hybridized carbon, the electronic properties of graphene oxide can be tuned from being and insulator to semi-conductor and to a semi-metal like graphene. Moreover, it has been shown recently both theoretically and experimentally, that upon a careful control of the functional groups such as –O– and –OH, the electronic properties of graphene oxide can be controlled and made to act as a photocatalyst which can be driven using visible light. It has been recently shown in a theoretical work that a ratio of 1 : 1 for –OH and –O– groups may possess the highest photocatalytic activity among pristine graphene and graphene oxide derivatives.[318] Furthermore, the performance impeding factors such as uneven distribution of metal oxide nanoparticles on graphene, large size of metal oxide nanoparticles and defects, restacking, aggregation of graphene sheets are still being looked into and there is a need for further

research to develop methods of preparation for composite which can provide products which can overcome these factors. While there have been few photocurrent measurement studies on the nature of interactions between composites and pollutants, the underlying mechanism of the enhancement in the photocatalytic activity of the metal oxide graphene composites is not fully understood. Detailed DFT based simulation and analysis of metal oxide semiconductors and graphene should be carried out to understand the nature of interactions between them. This also provides us with an opportunity to design and tailor "functional" materials based on theoretical analysis. So far DFT studies have been performed for composite of metal oxides such as TiO_2 and ZnO with graphene, similar to these studies, further DFT studies can be carried for the optimisation of density and position of the functional groups for various carbon support materials and their interaction with other metal oxide semiconductors also; thereby providing a complete optimisation of the composite.

Developing water treatment technologies based on metal oxide/graphene composite will be an interesting but difficult task for researchers since still there are few questions answers of which yet to be find out such as what will the eventual fate of these composite and to what extent these technologies and materials are environment friendly? This means recycling and disposal of these expired composites is also a big challenge. Strategies for recycling and disposal of used composites will develop concurrently along with their application in household water purification devises to avoid waste generation. The post treatment recovery of the composites from the water is crucial as these composites can potentially cross-contaminate the treated water. The composites of magnetic oxides with graphene can be a potential solution to this problem as magnetic materials can be easily separated out using an external magnet but most of the used magnetic oxides such as Fe_3O_4 and Fe_2O_3 do not exhibit significant photocatalytic activity and hence there is a need of designing metal oxides such as $ZnFe_2O_4$ and $BeFeO_3$ which can show both magnetic and photo-catalytic activity at the same time. Development of methods for the formation of composites of graphene with metal oxides without losing surface area of graphene significantly is also a major challenge in the designing of metal oxides/graphene composites based adsorbents. Though graphene metal oxide composites have shown immense possibilities as photocatalyst but still there are issues with these materials which need to be resolved such as the nature of chemical interaction or bonding metal oxides and graphene is not fully understood which must be thoroughly investigated to design more effective photocatalyst. There is a need of detailed studies on optimization of graphene content in the composite to achieve maximum output from these composites.

Adsorbents developed using metal oxide/graphene composites will have to compete with the activated carbons in term of cost and popularity. Few studies mentioned in this article have reported that metal oxide/graphene based composite can be utilized for selective adsorption of ions which is needed to be further investigate to design adsorbents which can have selectivity towards specific ions. Metal oxide/graphene composite based disinfectants are not well explored therefore detailed

studies about mechanism of action, effectiveness and toxicity profile are still being investigated. Water quality is quite a sensitive issue, as it is directly related to health of mankind therefore a thorough investigation of long term biological impact of metal oxide/graphene composite on different living beings is required prior to its bulk scale application as disinfectant. So far graphene based materials appear to be very promising for the water treatment application and has also been considered as materials of future for different other types of applications but still research on graphene is in nascent stage and there are lots of uncertainties so complete understanding of various phenomenon and properties related to graphene is needed to design more efficient devises. This review can be an input to the sum of efforts for understanding various phenomenon and properties related to the metal oxide/graphene composite particularly for those which are important from the point of view of water treatment.

Acknowledgements

References

1 H. W. Kroto, J. R. Heath, S. C. O'Brien, R. F. Curl and R. E. Smalley, *Nature*, 1985, **318**, 162–163.

2 S. Iijima, *Nature*, 1991, **354**, 56–58.

3 K. S. Novoselov, A. K. Geim, S. Morozov, D. Jiang, Y. Zhang, S. Dubonos, I. Grigorieva and A. Firsov, *Science*, 2004, **306**, 666–669.

4 C. Lee, X. Wei, J. W. Kysar and J. Hone, *Science*, 2008, **321**, 385–388.

5 Y. Zheng, N. Wei, Z. Fan, L. Xu and Z. Huang, *Nanotechnology*, 2011, **22**, 405701.

6 A. K. Geim and A. H. MacDonald, *Phys. Today*, 2007, **60**, 35–41.

7 A. S. Mayorov, R. V. Gorbachev, S. V. Morozov, L. Britnell, R. Jalil, L. A. Ponomarenko, P. Blake, K. S. Novoselov, K. Watanabe, T. Taniguchi and A. K. Giem, *Nano Lett.*, 2011, **11**, 2396–2399.

8 M. D. Stoller, S. Park, Y. Zhu, J. An and R. S. Ruoff, *Nano Lett.*, 2008, **8**, 3498–3502.

9 X. Li, Y. Zhu, W. Cai, M. Borysiak, B. Han, D. Chen, R. D. Piner, L. Colombo and R. S. Ruoff, *Nano Lett.*, 2009, **9**, 4359–4363.

10 J.-U. Lee, D. Yoon and H. Cheong, *Nano Lett.*, 2012, **12**, 4444–4448.

11 A. A. Balandin, *Nat. Mater.*, 2011, **10**, 569–581.

12 D. L. Nika, E. P. Pokatilov, A. S. Askerov and A. A. Balandin, *Phys. Rev. B: Condens. Matter Mater. Phys.*, 2009, **79**, 155413.

13 J. Moser, A. Barreiro and A. Bachtold, *Appl. Phys. Lett.*, 2007, **91**, 163513.

14 X. Wang, L. Zhi and K. Müllen, *Nano Lett.*, 2008, **8**, 323–327.

15 Z. Yin, S. Wu, X. Zhou, X. Huang, Q. Zhang, F. Boey and H. Zhang, *Small*, 2010, **6**, 307–312.

16 J. Wu, H. A. Becerril, Z. Bao, Z. Liu, Y. Chen and P. Peumans, *Appl. Phys. Lett.*, 2008, **92**, 263302.

17 P. Blake, P. D. Brimicombe, R. R. Nair, T. J. Booth, D. Jiang, F. Schedin, L. A. Ponomarenko, S. V. Morozov, H. F. Gleeson and E. W. Hill, *Nano Lett.*, 2008, **8**, 1704–1708.

18 M. F. El-Kady, V. Strong, S. Dubin and R. B. Kaner, *Science*, 2012, **335**, 1326–1330.

19 H. Wang, L.-F. Cui, Y. Yang, H. Sanchez Casalongue, J. T. Robinson, Y. Liang, Y. Cui and H. Dai, *J. Am. Chem. Soc.*, 2010, **132**, 13978–13980.

20 E. Yoo, J. Kim, E. Hosono, H.-s. Zhou, T. Kudo and I. Honma, *Nano Lett.*, 2008, **8**, 2277–2282.

21 M. Liang and L. Zhi, *J. Mater. Chem.*, 2009, **19**, 5871–5878.

22 F. Schedin, A. Geim, S. Morozov, E. Hill, P. Blake, M. Katsnelson and K. Novoselov, *Nat. MateR.*, 2007, **6**, 652–655.

23 Y. Shao, J. Wang, H. Wu, J. Liu, I. A. Aksay and Y. Lin, *Electroanalysis*, 2010, **22**, 1027–1036.

24 C. Shan, H. Yang, J. Song, D. Han, A. Ivaska and L. Niu, *Anal. Chem.*, 2009, **81**, 2378–2382.

25 K. C. Kemp, H. Seema, M. Saleh, N. H. Le, K. Mahesh, V. Chandra and K. S. Kim, *Nanoscale*, 2013, **5**, 3149–3171.

26 K. Lü, G. Zhao and X. Wang, *Chin. Sci. Bull.*, 2012, **57**, 1223–1234.

27 T. S. Sreeprasad and T. Pradeep, *Int. J. Mod. Phys. B*, 2012, **26**, 1242001.

28 Z. Yang, H. Yan, H. Yang, H. Li, A. Li and R. Cheng, *Water Res.*, 2013, **47**, 3037–3046.

29 A. K. Mishra and S. Ramaprabhu, *Desalination*, 2011, **282**, 39–45.

30 L. Fan, C. Luo, M. Sun, H. Qiu and X. Li, *Colloids Surf., B*, 2013, **103**, 601–607.

31 H. Wang, X. Yuan, Y. Wu, H. Huang, G. Zeng, Y. Liu, X. Wang, N. Lin and Y. Qi, *Appl. Surf. Sci.*, 2013, **279**, 432–440.

32 R. Li, L. Liu and F. Yang, *Chem. Eng. J.*, 2013, **229**, 460–468.

33 R. Haberl, *Water Sci. Technol.*, 1999, **40**, 11–17.

34 H. Bouwer, *Agricultural Water Management*, 2000, **45**, 217–228.

35 M. Razvigorova, T. Budinova, N. Petrov and V. Minkova, *Water Res.*, 1998, **32**, 2135–2139.

36 A. Bhatnagar, W. Hogland, M. Marques and M. Sillanpää, *Chem. Eng. J.*, 2012, **219**, 499–511.

37 M. J. McAllister, J.-L. Li, D. H. Adamson, H. C. Schniepp, A. A. Abdala, J. Liu, M. Herrera-Alonso, D. L. Milius, R. Car and R. K. Prud'homme, *Chem. Mater.*, 2007, **19**, 4396–4404.

38 A. Fujishima and K. Honda, *Nature*, 1972, **238**, 37–38.

39 D. Chatterjee and S. Dasgupta, *J. Photochem. Photobiol., C*, 2005, **6**, 186–205.

40 J.-M. Herrmann, *Catal. Today*, 1999, **53**, 115–129.

41 N. Khalid, Z. Hong, E. Ahmed, Y. Zhang, H. Chan and M. Ahmad, *Appl. Surf. Sci.*, 2012, **258**, 5827–5834.

42 B. Neppolian, A. Bruno, C. L. Bianchi and M. Ashokkumar, *Ultrason. Sonochem.*, 2012, **19**, 9–15.

43 Y. Tang, S. Luo, Y. Teng, C. Liu, X. Xu, X. Zhang and L. Chen, *J. Hazard.Mater.*, 2012, **241–242**, 323–330.

44 N. Shaari, S. Tan and A. Mohamed, *J. Rare Earths*, 2012, **30**, 651–658.

45 K. Zhang, F. J. Zhang, M. L. Chen and W. C. Oh, *Ultrason. Sonochem.*, 2011, **18**, 765–772.

46 Y. Gou, D. Chen and Z. Su, *Appl. Catal., A*, 2004, **261**, 15–18.

47 S. Wang, H. Sun, H. Ang and M. Tadé, *Chem. Eng. J.*, 2013, **226**, 336–347.

48 J. Theron, J. Walker and T. Cloete, *Crit. Rev. Microbiol.*, 2008, **34**, 43–69.

49 D. R. Dreyer, S. Park, C. W. Bielawski and R. S. Ruoff, *Chem. Soc. Rev.*, 2010, **39**, 228–240.

50 A. Farghali, M. Bahgat, W. El Rouby and M. Khedr, *J. Alloys Compd.*, 2012, **555**, 193–200.

51 T. Wu, X. Cai, S. Tan, H. Li, J. Liu and W. Yang, *Chem. Eng. J.*, 2011, **173**, 144–149.

52 D. Zhang, L. Fu, L. Liao, B. Dai, R. Zou and C. Zhang, *Electrochim. Acta*, 2012, **75**, 71–79.

53 Z.-H. Huang, X. Zheng, W. Lv, M. Wang, Q.-H. Yang and F. Kang, *Langmuir*, 2011, **27**, 7558–7562.

54 X. Deng, L. Lü, H. Li and F. Luo, *J. Hazard. Mater.*, 2010, **183**, 923–930.

55 C. J. Madadrang, H. Y. Kim, G. Gao, N. Wang, J. Zhu, H. Feng, M. Gorring, M. L. Kasner and S. Hou, *ACS Appl. Mater. Interfaces*, 2012, **4**, 1186–1193.

56 Y. Li, Q. Du, T. Liu, J. Sun, Y. Jiao, Y. Xia, L. Xia, Z. Wang, W. Zhang and K. Wang, *Mater. Res. Bull.*, 2012, **47**, 1898–1904.

57 X. Li and G. Chen, *Mater. Lett.*, 2009, **63**, 930–932.

58 J. Xu, L. Wang and Y. Zhu, *Langmuir*, 2012, **28**, 8418–8425.

59 Y. Wu, H. Luo, H. Wang, C. Wang, J. Zhang and Z. Zhang, *J. Colloid Interface Sci.*, 2013, **394**, 183–191.

60 L. Fan, C. Luo, X. Li, F. Lu, H. Qiu and M. Sun, *J. Hazard. Mater.*, 2012, **215**, 272–279.

61 L. Li, L. Fan, M. Sun, H. Qiu, X. Li, H. Duan and C. Luo, *Int. J. Biol. Macromol.*, 2013, **58**, 169–175.

62 J. Guo, R. Wang, W. W. Tjiu, J. Pan and T. Liu, *J. Hazard. Mater.*, 2012, **225**, 63–73.

63 Y.-P. Chang, C.-L. Ren, J.-C. Qu and X.-G. Chen, *Appl. Surf. Sci.*, 2012, **261**, 504–509.

64 X. Zhang, C. Cheng, J. Zhao, L. Ma, S. Sun and C. Zhao, *Chem. Eng. J.*, 2013, **215–216**, 72–81.

65 Y. Huang, M. Zeng, J. Ren, J. Wang, L. Fan and Q. Xu, *Colloids Surf., A*, 2012, **401**, 97–106.

66 L. Fan, C. Luo, M. Sun, X. Li and H. Qiu, *Colloids Surf., B*, 2013, **103**, 523–529.

67 G. Zhao, J. Li, X. Ren, C. Chen and X. Wang, *Environ. Sci. Technol.*, 2011, **45**, 10454–10462.

68 L. Hao, H. Song, L. Zhang, X. Wan, Y. Tang and Y. Lv, *J. Colloid Interface Sci.*, 2012, **369**, 381–387.

69 G. Williams, B. Seger and P. V. Kamat, *ACS Nano*, 2008, **2**, 1487–1491.

70 S. Liu, T. H. Zeng, M. Hofmann, E. Burcombe, J. Wei, R. Jiang, J. Kong and Y. Chen, *ACS Nano*, 2011, **5**, 6971–6980.

71 O. Akhavan and E. Ghaderi, *ACS Nano*, 2010, **4**, 5731–5736.

72 S. Liu, M. Hu, T. H. Zeng, R. Wu, R. Jiang, J. Wei, L. Wang, J. Kong and Y. Chen, *Langmuir*, 2012, **28**, 12364–12372.

73 O. Akhavan and E. Ghaderi, *Carbon*, 2012, **50**, 1853–1860.

74 M. Shi, J. Shen, H. Ma, Z. Li, X. Lu, N. Li and M. Ye, *Colloids Surf., A*, 2012, **405**, 30–37.

75 D. Fu, G. Han, Y. Chang and J. Dong, *Mater. Chem. Phys.*, 2012, **132**, 673–681.

76 W. MingYan, H. JunRao, T. Zhi-Wei, L. Wei-Hua and C. Jun, *J. Alloys Compd.*, 2013, **568**, 26–35.

77 Y. Fu and X. Wang, *Ind. Eng. Chem. Res.*, 2011, **50**, 7210–7218.

78 Y. Fu, Q. Chen, M. He, Y. Wan, X. Sun, H. Xia and X. Wang, *Ind. Eng. Chem. Res.*, 2012, **51**, 11700–11709.

79 E. Gao, W. Wang, M. Shang and J. Xu, *Phys. Chem. Chem. Phys.*, 2011, **13**, 2887–2893.

80 E. Lee, J.-Y. Hong, H. Kang and J. Jang, *J. Hazard. Mater.*, 2012, **219**, 13–18.

81 M. R. Hoffmann, S. T. Martin, W. Choi and D. W. Bahnemann, *Chem. Rev.*, 1995, **95**, 69–96.

82 R. Nainani, P. Thakur and M. Chaskar, *J. Mater. Sci. Eng. B*, 2012, **2**, 52–58.

83 W.-J. Yin, S. Chen, J.-H. Yang, X.-G. Gong, Y. Yan and S.-H. Wei, *Appl. Phys. Lett.*, 2010, **96**, 221901.

84 G. Yang, Z. Jiang, H. Shi, T. Xiao and Z. Yan, *J. Mater. Chem.*, 2010, **20**, 5301–5309.

85 W. Choi, A. Termin and M. R. Hoffmann, *J. Phys. Chem.*, 1994, **98**, 13669–13679.

86 I. N. Martyanov, S. Uma, S. Rodrigues and K. J. Klabunde, *Chem. Commun.*, 2004, 2476–2477.

87 V. Etacheri, M. K. Seery, S. J. Hinder and S. C. Pillai, *Adv. Funct. Mater.*, 2011, **21**, 3744–3752.

88 K. Li, T. Chen, L. Yan, Y. Dai, Z. Huang, J. Xiong, D. Song, Y. Lv and Z. Zeng, *Colloids Surf., A*, 2013, **422**, 90–99.

89 T. Jiang, L. Zhang, M. Ji, Q. Wang, Q. Zhao, X. Fu and H. Yin, *Particuology*, DOI: 10.1016/j.partic.2012.07.008.

90 K. Woan, G. Pyrgiotakis and W. Sigmund, *Adv. Mater.*, 2009, **21**, 2233–2239.

91 H. Zhang, X. Lv, Y. Li, Y. Wang and J. Li, *ACS Nano*, 2009, **4**, 380–386.

92 D.-H. Yoo, T. V. Cuong, V. H. Pham, J. S. Chung, N. T. Khoa, E. J. Kim and S. H. Hahn, *Curr. Appl. Phys.*, 2011, **11**, 805–808.

93 W. Wang, J. Yu, Q. Xiang and B. Cheng, *Appl. Catal., B*, 2012, **119–120**, 109–116.

94 Y. Wang, R. Shi, J. Lin and Y. Zhu, *Appl. Catal., B*, 2010, **100**, 179–183.

95 Y. Liang, H. Wang, H. S. Casalongue, Z. Chen and H. Dai, *Nano Res.*, 2010, **3**, 701–705.

96 T. Ghosh, K.-Y. Cho, K. Ullah, V. Nikam, C.-Y. Park, Z.-D. Meng and W.-C. Oh, *J. Ind. Eng. Chem.*, 2012, **19**, 797–805.

97 Y. Min, G. He, R. Li, W. Zhao, Y. Chen and Y. Zhang, *Sep. Purif. Technol.*, 2013, **106**, 97–104.

98 M. Shi, J. Shen, H. Ma, Z. Li, X. Lu, N. Li and M. Ye, *Colloids Surf., A*, 2012, **405**, 30–37.

99 S. Stankovich, D. A. Dikin, R. D. Piner, K. A. Kohlhaas, A. Kleinhammes, Y. Jia, Y. Wu, S. T. Nguyen and R. S. Ruoff, *Carbon*, 2007, **45**, 1558–1565.

100 X. Li, G. Zhang, X. Bai, X. Sun, X. Wang, E. Wang and H. Dai, *Nat. Nanotechnol.*, 2008, **3**, 538–542.

101 X. Zhu, Q. Liu, X. Zhu, C. Li, M. Xu and Y. Liang, *Int. J. Electrochem. Sci.*, 2012, **7**, 5172–5184.

102 Y. H. Ng, I. V. Lightcap, K. Goodwin, M. Matsumura and P. V. Kamat, *J. Phys. Chem. Lett.*, 2010, **1**, 2222–2227.

103 Y. Zhang, Z.-R. Tang, X. Fu and Y.-J. Xu, *ACS Nano*, 2010, **4**, 7303–7314.

104 S. Roy, N. Soin, R. Bajpai, D. S. Misra, J. A. McLaughlin and S. S. Roy, *J. Mater. Chem.*, 2011, **21**, 14725–14731.

105 M.-Q. Yang, N. Zhang and Y.-J. Xu, *ACS Appl. Mater. Interfaces*, 2013, **5**, 1156–1164.

106 Y. Zhang, Z.-R. Tang, X. Fu and Y.-J. Xu, *ACS Nano*, 2011, **5**, 7426–7435.

107 W. Geng, H. Liu and X. Yao, *Phys. Chem. Chem. Phys.*, 2013, **15**, 6025–6033.

108 W. Wang, C. Lu, Y. Ni and Z. Xu, *Appl. Catal., B*, 2013, **129**, 606–613.

109 N. Khalid, E. Ahmed, Z. Hong, Y. Zhang, M. Ullah and M. Ahmed, *Ceram. Int.*, 2013, **39**, 3569–3575.

110 S. Liu, H. Sun, S. Liu and S. Wang, *Chem. Eng. J.*, 2013, **214**, 298–303.

111 Z.-D. Meng, L. Zhu, T. Ghosh, C.-Y. Park, K. Ullah, V. Nikam and W.-C. Oh, *Bull. Korean Chem. Soc.*, 2012, **33**, 3761–3766.

112 A. A. Ismail, R. A. Geioushy, H. Bouzid, S. A. Al-Sayari, A. Al-Hajry and D. W. Bahnemann, *Appl. Catal., B*, 2013, **129**, 62–70.

113 H. Zhao, F. Su, X. Fan, H. Yu, D. Wu and X. Quan, *Chin. J. Catal.*, 2012, **33**, 777–782.

114 J. Guo, S. Zhu, Z. Chen, Y. Li, Z. Yu, Q. Liu, J. Li, C. Feng and D. Zhang, *Ultrason. Sonochem.*, 2011, **18**, 1082–1090.

115 N. Farhangi, R. R. Chowdhury, Y. Medina-Gonzalez, M. B. Ray and P. A. Charpentier, *Appl. Catal., B*, 2011, **110**, 25–32.

116 Z. Zhang, W. Yang, X. Zou, F. Xu, X. Wang, B. Zhang and J. Tang, *J. Colloid Interface Sci.*, 2012, **386**, 198–204.

117 Y. Min, K. Zhang, W. Zhao, F. Zheng, Y. Chen and Y. Zhang, *Chem. Eng. J.*, 2012, **193**, 203–210.

118 D. Wang, X. Li, J. Chen and X. Tao, *Chem. Eng. J.*, 2012, **198–199**, 547–554.

119 N. Khalid, E. Ahmed, Z. Hong, L. Sana and M. Ahmed, *Curr. Appl. Phys.*, 2013, **13**, 659–663.

120 N. Khalid, E. Ahmed, Z. Hong and M. Ahmad, *Appl. Surf. Sci.*, 2012, **263**, 254–259.

121 D. Zhao, G. Sheng, C. Chen and X. Wang, *Appl. Catal., B*, 2012, **111**, 303–308.

122 F. Wang and K. Zhang, *J. Mol. Catal. A: Chem.*, 2011, **345**, 101–107.

123 L. M. Pastrana-Martínez, S. Morales-Torres, A. G. Kontos, N. G. Moustakas, J. L. Faria, J. M. Doña-Rodríguez, P. Falaras and A. M. Silva, *Chem. Eng. J.*, 2012, **224**, 17–23.

124 Y.-p. Zhang, J.-j. Xu, Z.-h. Sun, C.-z. Li and C.-x. Pan, *Progress in Natural Science: Materials International*, 2011, **21**, 467–471.

125 S. Ghasemi, S. R. Setayesh, A. Habibi-Yangjeh, M. Hormozi-Nezhad and M. Gholami, *J. Hazard. Mater.*, 2012, **199**, 170–178.

126 G. Jiang, Z. Lin, C. Chen, L. Zhu, Q. Chang, N. Wang, W. Wei and H. Tang, *Carbon*, 2011, **49**, 2693–2701.

127 K. Zhang, K. C. Kemp and V. Chandra, *Mater. Lett.*, 2012, **81**, 127–130.

128 T.-D. Nguyen-Phan, V. H. Pham, E. W. Shin, H.-D. Pham, S. Kim, J. S. Chung, E. J. Kim and S. H. Hur, *Chem. Eng. J.*, 2011, **170**, 226–232.

129 Y. Min, K. Zhang, L. Chen, Y. Chen and Y. Zhang, *Synth. Met.*, 2012, **162**, 827–833.

130 X. Pu, D. Zhang, Y. Gao, X. Shao, G. Ding, S. Li and S. Zhao, *J. Alloys Compd.*, 2013, **551**, 382–388.

131 C. H. Kim, B.-H. Kim and K. S. Yang, *Carbon*, 2012, **50**, 2472–2481.

132 L. Zhu, T. Ghosh, C.-Y. Park, Z.-D. Meng and W.-C. Oh, *Chin. J. Catal.*, 2012, **33**, 1276–1283.

133 X. Liu, L. Pan, T. Lv and Z. Sun, *J. Colloid Interface Sci.*, 2012, **394**, 441–444.

134 G. Hu and B. Tang, *Mater. Chem. Phys.*, 2013, **138**, 608–614.

135 Z. Qianqian, B. Tang and H. Guoxin, *J. Hazard. Mater.*, 2011, **198**, 78–86.

136 L. M. Pastrana-Martínez, S. Morales-Torres, V. Likodimos, J. L. Figueiredo, J. L. Faria, P. Falaras and A. M. Silva, *Appl. Catal., B*, 2012, **123–124**, 241–256.

137 Z. Wang, F. Mao, X. Huang, Y. Huang, S. Feng, J. Yi, C. Zhang, H. Wei and S. Liu, *Rare Met.*, 2011, **30**, 271–275.

138 Y. Gao, X. Pu, D. Zhang, G. Ding, X. Shao and J. Ma, *Carbon*, 2012, **50**, 4093–4101.

139 H. Yun, T.-D. Nguyen-Phan, V. H. Pham, H. Kweon, J. S. Chung, B. Lee and E. W. Shin, *Mater. Res. Bull.*, 2012, **47**, 2988–2993.

140 K. Li, T. Chen, L. Yan, Y. Dai, Z. Huang, H. Guo, L. Jiang, X. Gao, J. Xiong and D. Song, *Catal. Commun.*, 2012, **28**, 196–201.

141 X. Pan, Y. Zhao, S. Liu, C. L. Korzeniewski, S. Wang and Z. Fan, *ACS Appl. Mater. Interfaces*, 2012, **4**, 3944–3950.

142 V. c. Štengl, D. Popelková and P. Vláčil, *J. Phys. Chem. C*, 2011, **115**, 25209–25218.

143 S. Anandan, T. Narasinga Rao, M. Sathish, D. Rangappa, I. Honma and M. Miyauchi, *ACS Appl. Mater. Interfaces*, 2013, **5**, 207–212.

144 T. Kamegawa, D. Yamahana and H. Yamashita, *J. Phys. Chem. C*, 2010, **114**, 15049–15053.

145 M. S. A. Sher Shah, A. R. Park, K. Zhang, J. H. Park and P. J. Yoo, *ACS Appl. Mater. Interfaces*, 2012, **4**, 3893–3901.

146 S. D. Perera, R. G. Mariano, K. Vu, N. Nour, O. Seitz, Y. Chabal and K. J. Balkus Jr, *ACS Catal.*, 2012, **2**, 949–956.

147 Y. Min, K. Zhang, L. Chen, Y. Chen and Y. Zhang, *Diamond Relat. Mater.*, 2012, **26**, 32–38.

148 X. Zhou, T. Shi and H. Zhou, *Appl. Surf. Sci.*, 2012, **258**, 6204–6211.

149 T. Xu, L. Zhang, H. Cheng and Y. Zhu, *Appl. Catal., B*, 2011, **101**, 382–387.

150 Z. Khan, T. R. Chetia, A. K. Vardhaman, D. Barpuzary, C. V. Sastri and M. Qureshi, *RSC Adv.*, 2012, **2**, 12122–12128.

151 X. An, C. Y. Jimmy, Y. Wang, Y. Hu, X. Yu and G. Zhang, *J. Mater. Chem.*, 2012, **22**, 8525–8531.

152 N. Yusoff, N. Huang, M. Muhamad, S. Kumar, H. Lim and I. Harrison, *Mater. Lett.*, 2013, **93**, 393–396.

153 Z. Gao, J. Liu, F. Xu, D. Wu, Z. Wu and K. Jiang, *Solid State Sci.*, 2012, **14**, 276–280.

154 Y. Yao, C. Xu, S. Yu, D. Zhang and S. Wang, *Ind. Eng. Chem. Res.*, 2013, **52**, 3637–3645.

155 S. Chandra, P. Das, S. Bag, R. Bhar and P. Pramanik, *Mater. Sci. Eng., B*, 2012, **177**, 855–861.

156 H. Seema, K. C. Kemp, V. Chandra and K. S. Kim, *Nanotechnology*, 2012, **23**, 355705.

157 X. Bai, L. Wang and Y. Zhu, *ACS Catal.*, 2012, **2**, 2769–2778.

158 P. Wang, Y. Ao, C. Wang, J. Hou and J. Qian, *Carbon*, 2012, **50**, 5256–5264.

159 Y. Yan, S. Sun, Y. Song, X. Yan, W. Guan, X. Liu and W. Shi, *J. Hazard. Mater.*, 2013, **250–251**, 106–114.

160 S. B. Gawande and S. R. Thakare, *Int. Nano Lett.*, 2013, **3**, 1–8.

161 Y. Fu, H. Chen, X. Sun and X. Wang, *Appl. Catal., B*, 2012, **111**, 280–287.

162 S. Liu, H. Sun, A. Suvorova and S. Wang, *Chem. Eng. J.*, 2013, **229**, 533–539.

163 J. Zhang, Z. Xiong and X. Zhao, *J. Mater. Chem.*, 2011, **21**, 3634–3640.

164 Z. Wang, Y. Du, F. Zhang, Z. Zheng, X. Zhang, Q. Feng and C. Wang, *Mater. Chem. Phys.*, 2013, **140**, 373–381.

165 W. Geng, X. Zhao, H. Liu and X. Yao, *J. Phys. Chem. C*, 2013, **117**, 10536–10544.

166 T.-T. Chen, I. Chang, M.-H. Yang, H.-T. Chiu and C.-Y. Lee, *Appl. Catal., B*, 2013, **142–143**, 442–449.

167 B. Li and H. Cao, *J. Mater. Chem.*, 2011, **21**, 3346–3349.

168 Q.-P. Luo, X.-Y. Yu, B.-X. Lei, H.-Y. Chen, D.-B. Kuang and C.-Y. Su, *J. Phys. Chem. C*, 2012, **116**, 8111–8117.

169 H. Fan, X. Zhao, J. Yang, X. Shan, L. Yang, Y. Zhang, X. Li and M. Gao, *Catal. Commun.*, 2012, **29**, 29–34.

170 X. Zhang, X. Quan, S. Chen and H. Yu, *Appl. Catal., B*, 2011, **105**, 237–242.

171 G. H. Rossetti, E. D. Albizzati and O. M. Alfano, *Ind. Eng. Chem. Res.*, 2002, **41**, 1436–1444.

172 B. Li, T. Liu, Y. Wang and Z. Wang, *J. Colloid Interface Sci.*, 2012, **377**, 114–121.

173 R. C. Pawar, D. Cho and C. S. Lee, *Curr. Appl. Phys.*, 2013, **13**, S50–S57.

174 L. Zhang, L. Du, X. Cai, X. Yu, D. Zhang, L. Liang, P. Yang, X. Xing, W. Mai, S. Tan, Y. Gu and J. Song, *Physica E*, 2013, **47**, 279–284.

175 G. Chen, M. Sun, Q. Wei, Y. Zhang, B. Zhu and B. Du, *J. Hazard. Mater.*, 2013, **244–245**, 86–93.

176 X. Yu, G. Zhang, H. Cao, X. An, Y. Wang, Z. Shu, X. An and F. Hua, *New J. Chem.*, 2012, **36**, 2593–2598.

177 Y.-L. Min, K. Zhang, Y.-C. Chen and Y.-G. Zhang, *Sep. Purif. Technol.*, 2012, **86**, 98–105.

178 S. B. Gawande and S. R. Thakare, *Int. Nano Lett.*, 2012, **2**, 1–7.

179 F. Zhou and Y. Zhu, *J. Adv. Ceram.*, 2012, **1**, 72–78.

180 M. Zhu, P. Chen and M. Liu, *Chin. Sci. Bull.*, 2013, **58**, 84–91.

181 N. P. Herring, S. H. Almahoudi, C. R. Olson and M. S. El-Shall, *J. Nanopart. Res.*, 2012, **14**, 1–13.

182 F. Zhou, R. Shi and Y. Zhu, *J. Mol. Catal. A: Chem.*, 2011, **340**, 77–82.

183 Z. Liu, W. Xu, J. Fang, X. Xu, S. Wu, X. Zhu and Z. Chen, *Appl. Surf. Sci.*, 2012, **259**, 441–447.

184 P. Wang, Y. Ao, C. Wang, J. Hou and J. Qian, *Carbon*, 2012, **50**, 5256–5264.

185 X. Zhang, X. Chang, M. Gondal, B. Zhang, Y. Liu and G. Ji, *Appl. Surf. Sci.*, 2012, **258**, 7826–7832.

186 H. Raj Pant, B. Pant, H. Joo Kim, A. Amarjargal, C. Hee Park, L. D. Tijing, E. Kyo Kim and C. Sang Kim, *Ceram. Int.*, 2013, **39**, 5083–5091.

187 Z. Ai, W. Ho and S. Lee, *J. Phys. Chem. C*, 2011, **115**, 25330–25337.

188 X. Yang, H. Cui, Y. Li, J. Qin, R. Zhang and H. Tang, *ACS Catal.*, 2013, **3**, 363–369.

189 Y. Min, F.-J. Zhang, W. Zhao, F. Zheng, Y. Chen and Y. Zhang, *Chem. Eng. J.*, 2012, **209**, 215–222.

190 M. Zhou, J. Yan and P. Cui, *Mater. Lett.*, 2012, **89**, 258–261.

191 Z. Chen, N. Zhang and Y.-J. Xu, *CrystEngComm*, 2013, **15**, 3022–3030.

192 T. Lv, L. Pan, X. Liu and Z. Sun, *Catal. Sci. Technol.*, 2012, **2**, 2297–2301.

193 Y. Yang, L. Ren, C. Zhang, S. Huang and T. Liu, *ACS Appl. Mater. Interfaces*, 2011, **3**, 2779–2785.

194 F. Xu, Y. Yuan, D. Wu, M. Zhao, Z. Gao and K. Jiang, *Mater. Res. Bull.*, 2013, **48**, 2066–2070.

195 H. R. Pant, C. H. Park, P. Pokharel, L. D. Tijing, D. S. Lee and C. S. Kim, *Powder Technol.*, 2013, **235**, 853–858.

196 L. Sun, R. Shao, L. Tang and Z. Chen, *J. Alloys Compd.*, 2013, **564**, 55–62.

197 S. Ameen, M. Shaheer Akhtar, H.-K. Seo and H. Shik Shin, *Mater. Lett.*, 2013, **100**, 261–265.

198 Y. Zhang, Z. Chen, S. Liu and Y.-J. Xu, *Appl. Catal., B*, 2013, **140–141**, 598–607.

199 H. Sun, S. Liu, S. Liu and S. Wang, *Appl. Catal., B*, 2014, **146**, 162–168.

200 Y. Liu, Y. Hu, M. Zhou, H. Qian and X. Hu, *Appl. Catal., B*, 2012, **125**, 425–431.

201 Y. Gong, X. Meng, C. Zou, Y. Yao, W. Fu, M. Wang, G. Yin, Z. Huang, X. Liao and X. Chen, *Mater. Lett.*, 2013, **106**, 171–174.

202 Y. Hou, X. Li, Q. Zhao and G. Chen, *Appl. Catal., B*, 2013, **142–143**, 80–88.

203 C. Wu, Y. Zhang, S. Li, H. Zheng, H. Wang, J. Liu, K. Li and H. Yan, *Chem. Eng. J.*, 2011, **178**, 468–474.

204 A. Wei, L. Xiong, L. Sun, Y. Liu, W. Li, W. Lai, X. Liu, L. Wang, W. Huang and X. Dong, *Mater. Res. Bull.*, 2013, **48**, 2855–2860.

205 S. Vijay Kumar, N. Huang, N. Yusoff and H. Lim, *Mater. Lett.*, 2013, **93**, 411–414.

206 D. Lu, Y. Zhang, S. Lin, L. Wang and C. Wang, *J. Alloys Compd.*, 2013, **579**, 336–342.

207 S. Bai, X. Shen, H. Lv, G. Zhu, C. Bao and Y. Shan, *J. Colloid Interface Sci.*, 2013, **405**, 1–9.

208 B. Zeng, X. Chen, X. Ning, C. Chen, W. Deng, Q. Huang and W. Zhong, *Appl. Surf. Sci.*, 2013, **276**, 482–486.

209 B. Li, T. Liu, L. Hu and Y. Wang, *J. Phys. Chem. Solids*, 2013, **74**, 635–640.

210 T. Xian, H. Yang, L. J. Di and J. F. Dai, *Res. Chem. Intermed.*, 2013, 1–9.

211 Y. Fang, R. Wang, G. Jiang, H. Jin, Y. Wang, X. Sun, S. Wang and T. Wang, *Bull. Mater. Sci.*, 2012, **35**, 495–499.

212 T. Kavitha, A. I. Gopalan, K.-P. Lee and S.-Y. Park, *Carbon*, 2012, **50**, 2994–3000.

213 D. Fu, G. Han, F. Yang, T. Zhang, Y. Chang and F. Liu, *Appl. Surf. Sci.*, 2013, **283**, 654–659.

214 D.-H. Yoo, T. V. Cuong, V. H. Luan, N. T. Khoa, E. J. Kim, S. H. Hur and S. H. Hahn, *J. Phys. Chem. C*, 2012, **116**, 7180–7184.

215 Q. Zhang, C. Tian, A. Wu, T. Tan, L. Sun, L. Wang and H. Fu, *J. Mater. Chem.*, 2012, **22**, 11778–11784.

216 X. Bai, L. Wang, R. Zong, Y. Lv, Y. Sun and Y. Zhu, *Langmuir*, 2013, **29**, 3097–3105.

217 C. Wen, F. Liao, S. Liu, Y. Zhao, Z. Kang, X. Zhang and M. Shao, *Chem. Commun.*, 2013, **49**, 3049–3051.

218 X. Chang, L. Dong, Y. Yin and S. Sun, *RSC Adv.*, 2013, **3**, 15005–15013.

219 A. Sun, H. Chen, C. Song, F. Jiang, X. Wang and Y. Fu, *RSC Adv.*, 2013, **3**, 4332–4340.

220 S. Sun, W. Wang and L. Zhang, *J. Phys. Chem. C*, 2013, **117**, 9113–9120.

221 S. Song, W. Gao, X. Wang, X. Li, D. Liu, Y. Xing and H. Zhang, *Dalton Trans.*, 2012, **41**, 10472–10476.

222 R. Huang, H. Ge, X. Lin, Y. Guo, R. Yuan, X. Fu and Z. Li, *RSC Adv.*, 2013, **3**, 1235–1242.

223 X. Tu, S. Luo, G. Chen and J. Li, *Chem.–Eur. J.*, 2012, **18**, 14359–14366.

224 Y. T. Liang, B. K. Vijayan, K. A. Gray and M. C. Hersam, *Nano Lett.*, 2011, **11**, 2865–2870.

225 G. K. Ramesha, A. Vijaya Kumara, H. B. Muralidhara and S. Sampath, *J. Colloid Interface Sci.*, 2011, **361**, 270–277.

226 J. N. Tiwari, K. Mahesh, N. H. Le, K. C. Kemp, R. Timilsina, R. N. Tiwari and K. S. Kim, *Carbon*, 2013, **56**, 173–182.

227 Z. Li, F. Chen, L. Yuan, Y. Liu, Y. Zhao, Z. Chai and W. Shi, *Chem. Eng. J.*, 2012, **210**, 539–546.

228 S. Bai, X. Shen, G. Zhu, A. Yuan, J. Zhang, Z. Ji and D. Qiu, *Carbon*, 2013, **60**, 157–168.

229 O. G. Apul, Q. Wang, Y. Zhou and T. Karanfil, *Water Res.*, 2013, **47**, 1648–1654.

230 Z. Pei, L. Li, L. Sun, S. Zhang, X.-q. Shan, S. Yang and B. Wen, *Carbon*, 2013, **51**, 156–163.

231 X. Wen, D. Zhang, T. Yan, J. Zhang and L. Shi, *J. Mater. Chem. A*, 2013, **1**, 12334–12344.

232 D. Zhang, X. Wen, L. Shi, T. Yan and J. Zhang, *Nanoscale*, 2012, **4**, 5440–5446.

233 H. Wang, D. Zhang, T. Yan, X. Wen, J. Zhang, L. Shi and Q. Zhong, *J. Mater. Chem. A*, 2013, **1**, 11778–11789.

234 H. Wang, D. Zhang, T. Yan, X. Wen, L. Shi and J. Zhang, *J. Mater. Chem.*, 2012, **22**, 23745–23748.

235 D. Zhang, T. Yan, L. Shi, Z. Peng, X. Wen and J. Zhang, *J. Mater. Chem.*, 2012, **22**, 14696–14704.

236 W. Lu, Y. Wu, J. Chen and Y. Yang, *CrystEngComm*, 2013, DOI: 10.1039/c3ce41833b.

237 P. Zong, S. Wang, Y. Zhao, H. Wang, H. Pan and C. He, *Chem. Eng. J.*, 2013, **220**, 45–52.

238 Q. Wu, G. Zhao, C. Feng, C. Wang and Z. Wang, *J. Chromatogr., A*, 2011, **1218**, 7936–7942.

239 C. Wang, C. Feng, Y. Gao, X. Ma, Q. Wu and Z. Wang, *Chem. Eng. J.*, 2011, **173**, 92–97.

240 V. Chandra, J. Park, Y. Chun, J. W. Lee, I.-C. Hwang and K. S. Kim, *ACS Nano*, 2010, **4**, 3979–3986.

241 M. Liu, C. Chen, J. Hu, X. Wu and X. Wang, *J. Phys. Chem. C*, 2011, **115**, 25234–25240.

242 J. Zhu, S. Wei, H. Gu, S. B. Rapole, Q. Wang, Z. Luo, N. Haldolaarachchige, D. P. Young and Z. Guo, *Environ. Sci. Technol.*, 2012, **46**, 977–985.

243 B. Alyüz and S. Veli, *J. Hazard. Mater.*, 2009, **167**, 482–488.

244 A.-H. Chen, S.-C. Liu, C.-Y. Chen and C.-Y. Chen, *J. Hazard. Mater.*, 2008, **154**, 184–191.

245 X. Yang, J. Li, T. Wen, X. Ren, Y. Huang and X. Wang, *Colloids Surf., A*, 2013, **422**, 118–125.

246 F. He, J. Fan, D. Ma, L. Zhang, C. Leung and H. L. Chan, *Carbon*, 2010, **48**, 3139–3144.

247 H. Sun, L. Cao and L. Lu, *Nano Res.*, 2011, **4**, 550–562.

248 N. Li, M. Zheng, X. Chang, G. Ji, H. Lu, L. Xue, L. Pan and J. Cao, *J. Solid State Chem.*, 2011, **184**, 953–958.

249 G. Zhao, S. Song, C. Wang, Q. Wu and Z. Wang, *Anal. Chim. Acta*, 2011, **708**, 155–159.

250 Y.-B. Luo, Z.-G. Shi, Q. Gao and Y.-Q. Feng, *J. Chromatogr., A*, 2011, **1218**, 1353–1358.

251 W. Wang, R. Ma, Q. Wu, C. Wang and Z. Wang, *Talanta*, 2013, **109**, 133–140.

252 R.-P. Liang, C.-M. Liu, X.-Y. Meng, J.-W. Wang and J.-D. Qiu, *J. Chromatogr., A*, 2012, **1266**, 95–102.

253 J. Wang, T. Tsuzuki, B. Tang, X. Hou, L. Sun and X. Wang, *ACS Appl. Mater. Interfaces*, 2012, **4**, 3084–3090.

254 M. Seredych and T. J. Bandosz, *Microporous Mesoporous Mater.*, 2012, **150**, 55–63.

255 Y. Ren, N. Yan, J. Feng, J. Ma, Q. Wen, N. Li and Q. Dong, *Mater. Chem. Phys.*, 2012, **136**, 538–544.

256 E. Zong, D. Wei, H. Wan, S. Zheng, Z. Xu and D. Zhu, *Chem. Eng. J.*, 2013, **221**, 193–203.

257 Z.-Q. Zhao, X. Chen, Q. Yang, J.-H. Liu and X.-J. Huang, *Chem. Commun.*, 2012, **48**, 2180–2182.

258 Y.-C. Lee and J.-W. Yang, *J. Ind. Eng. Chem.*, 2012, **18**, 1178–1185.

259 X. Luo, C. Wang, L. Wang, F. Deng, S. Luo, X. Tu and C. Au, *Chem. Eng. J.*, 2013, **220**, 98–106.

260 Y. Li, Q. Du, J. Wang, T. Liu, J. Sun, Y. Wang, Z. Wang, Y. Xia and L. Xia, *J. Fluorine Chem.*, 2013, **148**, 67–73.

261 Y. Ren, N. Yan, J. Feng, J. Ma, Q. Wen, N. Li and Q. Dong, *Mater. Chem. Phys.*, 2012, **136**, 538–544.

262 Y. Ren, N. Yan, Q. Wen, Z. Fan, T. Wei, M. Zhang and J. Ma, *Chem. Eng. J.*, 2011, **175**, 1–7.

263 L. Ai, C. Zhang and Z. Chen, *J. Hazard. Mater.*, 2011, **192**, 1515–1524.

264 X. Yuan, Y. Wang, J. Wang, C. Zhou, Q. Tang and X. Rao, *Chem. Eng. J.*, 2013, **221**, 204–213.

265 S. Zeng, N. Gan, R. Weideman-Mera, Y. Cao, T. Li and W. Sang, *Chem. Eng. J.*, 2013, **218**, 108–115.

266 Q. Han, Z. Wang, J. Xia, S. Chen, X. Zhang and M. Ding, *Talanta*, 2012, **101**, 388–395.

267 K. Zhang, V. Dwivedi, C. Chi and J. Wu, *J. Hazard. Mater.*, 2010, **182**, 162–168.

268 Q. Wu, C. Feng, C. Wang and Z. Wang, *Colloids Surf., B*, 2013, **101**, 210–214.

269 X. Luo, C. Wang, S. Luo, R. Dong, X. Tu and G. Zeng, *Chem. Eng. J.*, 2012, **187**, 45–52.

270 L. Li, L. Fan, M. Sun, H. Qiu, X. Li, H. Duan and C. Luo, *Colloids Surf., B*, 2013, **107**, 76–83.

271 T. Sreeprasad, S. M. Maliyekkal, K. Lisha and T. Pradeep, *J. Hazard. Mater.*, 2011, **186**, 921–931.

272 T.-D. Nguyen-Phan, V. H. Pham, E. J. Kim, E.-S. Oh, S. H. Hur, J. S. Chung, B. Lee and E. W. Shin, *Appl. Surf. Sci.*, 2012, **258**, 4551–4557.

273 S. Bai, X. Shen, X. Zhong, Y. Liu, G. Zhu, X. Xu and K. Chen, *Carbon*, 2012, **50**, 2337–2346.

274 D. Nandi, K. Gupta, A. K. Ghosh, A. De, S. Banerjee and U. C. Ghosh, *J. Nanopart. Res.*, 2012, **14**, 1–14.

275 J. Li, S. Zhang, C. Chen, G. Zhao, X. Yang, J. Li and X. Wang, *ACS Appl. Mater. Interfaces*, 2012, **4**, 4991–5000.

276 J.-H. Deng, X.-R. Zhang, G.-M. Zeng, J.-L. Gong, Q.-Y. Niu and J. Liang, *Chem. Eng. J.*, 2013, **226**, 189–200.

277 Y. Lin, S. Xu and L. Jia, *Chem. Eng. J.*, 2013, **225**, 679–685.

278 X.-j. Hu, Y.-g. Liu, H. Wang, A.-w. Chen, G.-m. Zeng, S.-m. Liu, Y.-m. Guo, X. Hu, T.-t. Li, Y.-q. Wang, L. Zhou and S.-h. Liu, *Sep. Purif. Technol.*, 2013, **108**, 189–195.

279 Y. Tang, H. Guo, L. Xiao, S. Yu, N. Gao and Y. Wang, *Colloids Surf., A*, 2013, **424**, 74–80.

280 Y. Yao, S. Miao, S. Yu, L. Ping Ma, H. Sun and S. Wang, *J. Colloid Interface Sci.*, 2012, **379**, 20–26.

281 G. Gollavelli, C.-C. Chang and Y.-C. Ling, *ACS Sustainable Chem. Eng.*, 2013, **1**, 462–472.

282 T. Wen, X. Wu, X. Tan, X. Wang and A. Xu, *ACS Appl. Mater. Interfaces*, 2013, **5**, 3304–3311.

283 N. A. Travlou, G. Z. Kyzas, N. K. Lazaridis and E. A. Deliyanni, *Langmuir*, 2013, **29**, 1657–1668.

284 W. Fan, W. Gao, C. Zhang, W. W. Tjiu, J. Pan and T. Liu, *J. Mater. Chem.*, 2012, **22**, 25108–25115.

285 G. Xie, P. Xi, H. Liu, F. Chen, L. Huang, Y. Shi, F. Hou, Z. Zeng, C. Shao and J. Wang, *J. Mater. Chem.*, 2012, **22**, 1033–1039.

286 M. Liu, T. Wen, X. Wu, C. Chen, J. Hu, J. Li and X. Wang, *Dalton Trans.*, 2013, **42**, 14710–14717.

287 Z. Geng, Y. Lin, X. Yu, Q. Shen, L. Ma, Z. Li, N. Pan and X. Wang, *J. Mater. Chem.*, 2012, **22**, 3527–3535.

288 X. Yang, C. Chen, J. Li, G. Zhao, X. Ren and X. Wang, *RSC Adv.*, 2012, **2**, 8821–8826.

289 G. Kyzas, N. Travlou, O. Kalogirou and E. Deliyanni, *Materials*, 2013, **6**, 1360–1376.

290 K. Krishnamoorthy, M. Veerapandian, L.-H. Zhang, K. Yun and S. J. Kim, *J. Phys. Chem. C*, 2012, **116**, 17280–17287.

291 V. C. Sanchez, A. Jachak, R. H. Hurt and A. B. Kane, *Chem. Res. Toxicol.*, 2011, **25**, 15–34.

292 F. Ahmed and D. F. Rodrigues, *J. Hazard. Mater.*, 2013, **256–257**, 33–39.

293 J. A. Nam, A.-A. Nahain, S. M. Kim, I. In and S. Y. Park, *Acta Biomater.*, 2013, **9**, 7996–8003.

294 S. Gurunathan, J. W. Han, A. A. Dayem, V. Eppakayala, M.-R. Park, D.-N. Kwon and J.-H. Kim, *J. Ind. Eng. Chem.*, 2013, **19**, 1280–1288.

295 O. Akhavan, E. Ghaderi and A. Esfandiar, *J. Phys. Chem. B*, 2011, **115**, 6279–6288.

296 O. N. Ruiz, K. A. S. Fernando, B. Wang, N. A. Brown, P. G. Luo, N. D. McNamara, M. Vangsness, Y.-P. Sun and C. E. Bunker, *ACS Nano*, 2011, **5**, 8100–8107.

297 G. Jia, H. Wang, L. Yan, X. Wang, R. Pei, T. Yan, Y. Zhao and X. Guo, *Environ. Sci. Technol.*, 2005, **39**, 1378–1383.

298 H. Wang, J. Wang, X. Deng, H. Sun, Z. Shi, Z. Gu, Y. Liu and Y. Zhaoc, *J. Nanosci. Nanotechnol.*, 2004, **4**, 1019–1024.

299 O. Akhavan and E. Ghaderi, *J. Phys. Chem. C*, 2009, **113**, 20214–20220.

300 J. Liu, L. Liu, H. Bai, Y. Wang and D. D. Sun, *Appl. Catal., B*, 2011, **106**, 76–82.

301 B. Cao, S. Cao, P. Dong, J. Gao and J. Wang, *Mater. Lett.*, 2013, **93**, 349–352.

302 P. Gao, J. Liu, D. D. Sun and W. Ng, *J. Hazard. Mater.*, 2013, **250–251**, 412–420.

303 L. Liu, J. Liu and D. D. Sun, *Catal. Sci. Technol.*, 2012, **2**, 2525–2532.

304 Y. Zhang, Y. Zhu, J. Yu, D. Yang, T. W. Ng, P.-K. Wong and J. Yu, *Nanoscale*, 2013, **5**, 6307–6310.

305 O. Akhavan, M. Choobtashani and E. Ghaderi, *J. Phys. Chem. C*, 2012, **116**, 9653–9659.

306 O. Akhavan, E. Ghaderi and K. Rahimi, *J. Mater. Chem.*, 2012, **22**, 23260–23266.

307 J. Ma, J. Zhang, Z. Xiong, Y. Yong and X. Zhao, *J. Mater. Chem.*, 2011, **21**, 3350–3352.

308 V. H. Nguyen, B. Kim, Y.-L. Jo and J.-J. Shim, *J. Supercrit. Fluids*, 2012, **72**, 28–35.

309 B. Jiang, C. Tian, G. Song, W. Chang, G. Wang, Q. Wu and H. Fu, *J. Mater. Sci.*, 2013, **48**, 1980–1985.

310 J. Tang, Q. Chen, L. Xu, S. Zhang, L. Feng, L. Cheng, H. Xu, Z. Liu and R. Peng, *ACS Appl. Mater. Interfaces*, 2013, **5**, 3867–3874.

311 J. Shen, T. Li, M. Shi, N. Li and M. Ye, *Mater. Sci. Eng., C*, 2012, **32**, 2042–2047.

312 N. Soin, S. S. Roy, T. H. Lim and J. A. D. McLaughlin, *Mater. Chem. Phys.*, 2011, **129**, 1051–1057.

313 N. Soin, S. S. Roy, C. O'Kane, J. A. D. McLaughlin, T. H. Lim and C. J. D. Hetherington, *CrystEngComm*, 2011, **13**, 312–318.

314 Y. Shen and A. C. Lua, *Sci. Rep.*, 2013, **3**, 3037.

315 H. Zhang, X. Zhang, X. Sun, D. Zhang, H. Lin, C. Wang, H. Wang and Y. Ma, *ChemSusChem*, 2013, **6**, 1084–1090.

316 Y. Wu, B. Wang, Y. Ma, Y. Huang, N. Li, F. Zhang and Y. Chen, *Nano Res.*, 2010, **3**, 661–669.

317 L. Liu, Z. Xiong, D. Hu, G. Wu and P. Chen, *Chem. Commun.*, 2013, **49**, 7890–7892.

318 X. Jiang, J. Nisar, B. Pathak, J. Zhao and R. Ahuja, *J. Catal.*, 2013, **299**, 204–209.

319 N. Yang, Y. Liu, H. Wen, Z. Tang, H. Zhao, Y. Li and D. Wang, *ACS Nano*, 2013, **7**, 1504–1512.